Inhibition of APE1-endonuclease activity affects cell metabolism in colon cancer cells via a p53-dependent pathway

Authored by: Marta Codrich[1], Marina Comelli[2], Matilde Clarissa Malfatti[1], Catia Mio[3], Dilara Ayyildiz[1], Chi Zhang[4], Mark R. Kelley[5], Giovanni Terrosu[6], Carlo EM Pucillo[7] & Gianluca Tell[1]

Highlights

- APE1 is overexpressed in colorectal cancer
- The APE1-endonuclease inhibitor (Compound #3) promotes p53 activation in HCT-116 colon cancer cell line.
- Compound #3 triggers p53-mediated effects on cell metabolism in HCT-116 colon cancer cell line.
- Compound #3 affects mitochondrial activity and sensitises cells to genotoxic treatment in a p53-dependent manner.
- 3D organoids derived from colorectal cancer patients are susceptible to Compound #3 in a p53-status correlated manner.
- Bioinformatics analyses support the hypothesis to target mitochondrial function in cancer cells through APE1-endonuclease inhibitors.
- Further studies are needed to test the possibility to target the endonuclease activity of APE1 in colorectal cancer.

This is the author's manuscript of the article published in final edited form as:

Codrich, M., Comelli, M., Malfatti, M. C., Mio, C., Ayyildiz, D., Zhang, C., … Tell, G. (2019). Inhibition of APE1-endonuclease activity affects cell metabolism in colon cancer cells via a p53-dependent pathway. DNA Repair, 82, 102675. https://doi.org/10.1016/j.dnarep.2019.102675

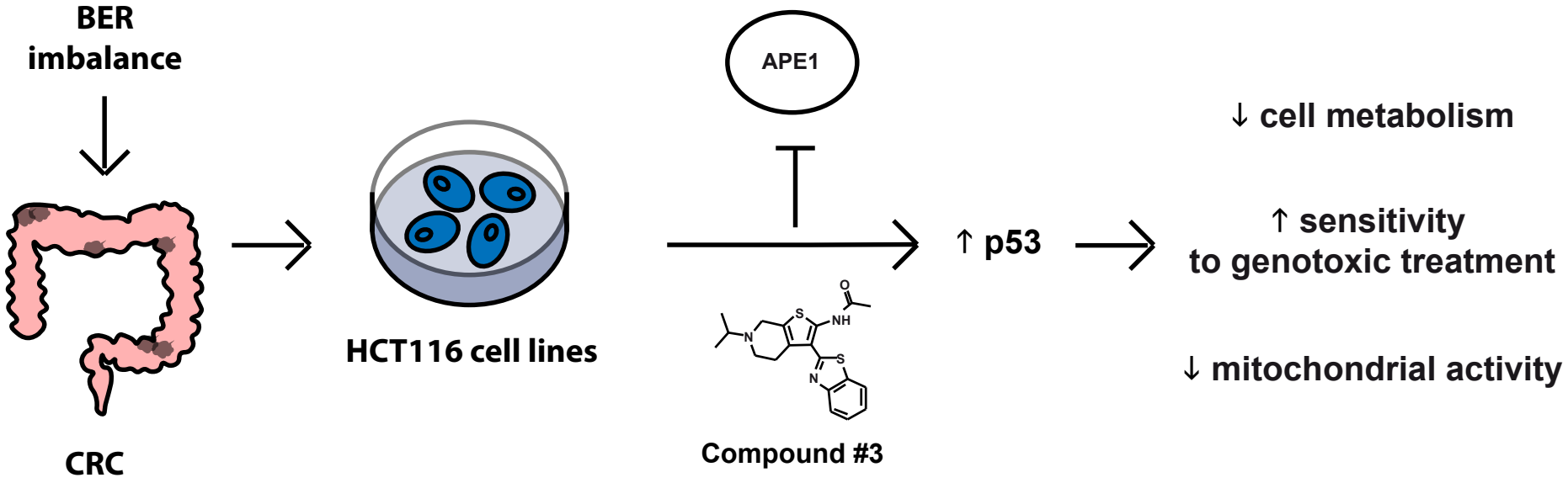
BER
imbalance
CRC
HCT116 cell lines
APE1
Compound #3
↑ p53
↓ cell metabolism
↑ sensitivity
to genotoxic treatment
↓ mitochondrial activity

Inhibition of APE1-endonuclease activity affects cell metabolism in colon cancer cells via a p53-dependent pathway

Marta Codrich[1], Marina Comelli[2], Matilde Clarissa Malfatti[1], Catia Mio[3], Dilara Ayyildiz[1], Chi Zhang[4], Mark R. Kelley[5], Giovanni Terrosu[6], Carlo EM Pucillo[7] & Gianluca Tell[1]

[1] Laboratory of Molecular Biology and DNA repair, Department of Medicine, University of Udine, Udine, 33100, Italy

[2] Laboratory of Bioenergetics, Department of Medicine, University of Udine, Udine, 33100, Italy

[3] Institute of Medical Genetics, Department of Medicine, University of Udine, Udine, 33100, Italy

[4] Department of Medical and Molecular Genetics, Center for Computational Biology and Bioinformatics, Indiana University, School of Medicine, Indianapolis, IN 46202, USA

[5] Herman B Wells Center for Pediatric Research, Department of Pediatrics and Pharmacology & Toxicology, Indiana University, School of Medicine, Indianapolis, IN 46202, USA

[6] General Surgery and Transplantation Unit, Department of Medicine, University of Udine, Udine, 33100, Italy

[7] Laboratory of Immunology, Department of Medicine, University of Udine, Udine, 33100, Italy

Corresponding Author:

Prof. Gianluca Tell, Head of the Laboratory of Molecular Biology and DNA repair, Department of Medicine, University of Udine, Piazzale M. Kolbe 4, 33100 Udine, Italy, Tel:+39 0432 494311, Fax: +39 0432 494301, gianluca.tell@uniud.it

Abstract

The pathogenesis of colorectal cancer (CRC) involves different mechanisms, such as genomic and microsatellite instabilities. Recently, a contribution of the base excision repair (BER) pathway in CRC pathology has been emerged. In this context, the involvement of APE1 in the BER pathway and in the transcriptional regulation of genes implicated in tumor progression strongly correlates with chemoresistance in CRC and in more aggressive cancers. In addition, the APE1 interactome is emerging as an important player in tumor progression, as demonstrated by its interaction with Nucleophosmin (NPM1). For these reasons, APE1 is becoming a promising target in cancer therapy and a powerful prognostic and predictive factor in several cancer types. Thus, specific APE1 inhibitors have been developed targeting: i) the endonuclease activity; ii) the redox function and iii) the APE1-NPM1 interaction. Furthermore, mutated p53 is a common feature of advanced CRC. The relationship between APE1 inhibition and p53 is still completely unknown. Here, we demonstrated that the inhibition of the endonuclease activity of APE1 triggers p53-mediated effects on cell metabolism in HCT-116 colon cancer cell line. In particular, the inhibition of the endonuclease activity, but not of the redox function or of the interaction with NPM1, promotes p53 activation in parallel to sensitization of p53-expressing HCT-116 cell line to genotoxic treatment. Moreover, the endonuclease inhibitor affects mitochondrial activity in a p53-dependent manner. Finally, we demonstrated that 3D organoids derived from CRC patients are susceptible to APE1-endonuclease inhibition in a p53-status correlated manner, recapitulating data obtained with HCT-116 isogenic cell lines. These findings suggest the importance of further studies aimed at testing the possibility to target the endonuclease activity of APE1 in CRC.

Keywords: colorectal cancer, BER, APE1, APE1-inhibitors, p53, organoids

1. Introduction

Colorectal cancer (CRC) is considered the third most common cancer and the fourth most common cause of cancer-related death worldwide [1]. CRC is a multistep process involving a series of histo-morphological and genetic changes, that accumulate over time in the epithelial layer of the intestinal tract. Interestingly, genetic and epigenetic modifications lead to the activation of oncogenes and/or the inactivation of tumor suppressor genes, as formulated by Volgestein and Fearon [2,3]. Both genetic and environmental factors are essential in the etiology of the disease. About 70% of CRC patients suffer from a sporadic form, whereas 10-30% present a familial predisposition and only 5-7% exhibit an inherited trait [4]. However, the most common, often overlapping, mechanisms involved in the pathogenesis of CRC are represented by the chromosome and microsatellite instabilities, the CpG island methylator phenotype and the deletion of the long arm of chromosome 18 [1,5]. In the landscape of chromosome instability, the most common mutations occur in specific tumor suppressor genes (e.g. *APC*, *PTEN*, *SMAD4*, *TGFBR2*, *TP53*) or oncogenes (e.g. *BRAF*, *KRAS*, *PIK3CA*). Recently, the involvement of DNA repair genes has been demonstrated to be associated with the pathogenesis of CRC [6–8]. In particular, both endogenous (e.g. metabolic activity of the cells) and exogenous factors (e.g. food intake) are involved in DNA damage, which requires the activation of the DNA repair mechanisms. In particular, the base excision repair (BER) pathway is involved in repairing DNA chemical modifications, such as deamination, oxidation, and alkylation [9]. Interestingly, BER has been found altered in CRC, as demonstrated by the presence of single nucleotide polymorphisms (SNPs) in several BER genes including DNA glycosylases, apurinic/apyrimidinic endonuclease 1 (APE1) and DNA Polymerase β (Pol β) [10]. In BER, APE1 cleaves the DNA phosphodiester backbone on the 5′ side of an abasic apurinic/apyrimidinic (AP) site, previously produced by the action of damage-specific glycosylases, generating a nick in the DNA and leaving 3′ hydroxyl and 5′ dRP free termini,

79 which are processed and replaced by a correct nucleotide by Pol β [11]. Recent molecular
80 snapshots of the endonuclease-reaction clearly defined the APE1 catalytic mechanism of
81 action [12]. The catalytic site of the enzymes involves a Mg^{2+} ion coordinated by Asp70,
82 Glu96 and a water molecule in contact with non-bridging oxygen of the phosphate.
83 Additionally, the nucleophilic water is in position for in-line attack of the phosphorus atom
84 and is coordinated by Asn212 and Asp210. APE1 is also endowed of an exonuclease activity
85 through the removal of 3' end groups of a mismatched or DNA damaged bases to generate
86 substrates that are processed by the downstream repair enzymes [13]. Recently, we
87 demonstrated that APE1 plays an important role in the recognition and processing of ribose
88 monophosphate AP sites and oxidized ribonucleotides embedded in DNA through a
89 classical AP endonuclease activity and a nucleotide incision repair (NIR) activity,
90 respectively [14].
91 As widely described, APE1 is implicated in cancer gene expression regulation due to its role
92 as a redox co-activator of several transcription factors, such as Egr-1, NF-κB, p53, STAT3,
93 HIF-1α, CREB, AP-1, and Pax-5/8 [15]. APE1 is considered as a unique nuclear redox-
94 signaling factor bearing seven Cys residues. Three of the Cys residues, C65, C93, and C99,
95 are essential for its redox activity, that involves a redox cycle through the potential formation
96 of intermolecular disulfide bonds with the protein target [16–20]. While C65 acts as the
97 nucleophilic cysteine, C93 and C99 likely play roles in resolving disulfide bonds that are
98 formed in APE1 upon oxidation. Structural studies demonstrated that APE1 exists in both
99 native and partially unfolded conformations, controlled by Thioredoxin (TRX) [16], in which
100 the partially unfolded state of APE1 represents the redox active intermediate of the enzyme.
101 Recently, it has been demonstrated that APE1 is not only involved in DNA repair
102 mechanisms and transcriptional regulation, but also in miRNA metabolism [21].
103 Furthermore, the interaction between APE1 and Nucleophosmin (NPM1) is essential for the
104 subcellular localization of APE1 modulating its endonuclease activity [22]. Interestingly, this

105 interaction was found altered in ovarian cancer promoting tumor aggressiveness and
106 resistance. Finally, it has been demonstrated that in the majority of cases, there is a positive
107 correlation between upregulated expression of APE1 and the development of several
108 tumors, such as: colon [23,24], breast [25], hepatic [26], prostate [27], pancreatic [28],
109 ovarian [29], lung cancers [30], leukemias [31] and many others [32]. Furthermore, APE1
110 overexpression is associated with the onset of chemoresistance phenomena [22]. For these
111 reasons, APE1 is considered a promising prognostic and predictive biomarker [33] and
112 several strategies have been developed to inhibit its functions in cancer cells [34], leading
113 to the development of ongoing clinical trials.
114 In recent years, a great effort has been put in the development of specific inhibitors targeting
115 the different functions of APE1, i.e. Compound #3, APX2009, Spiclomazine, Fiduxosin and
116 SB206553. Compound #3 blocks the endonuclease activity of APE1 acting as a competitive
117 inhibitor by binding the active site of the enzyme and consequently leading to a decrease of
118 APE1-DNA complex formation in a dose-dependent manner [35]. The inhibition promotes,
119 in turn, an increase of the unrepaired AP sites accumulation in genomic DNA, that, in
120 combination with an alkylating agent treatment, such as methyl methanesulfonate (MMS),
121 induces high levels of cellular death [36,37]. APX2009, an APE1 specific redox inhibitor, is
122 the second generation molecules of the drug APX3330, previously named E3330 [38].
123 APX3330 inhibits the activator function of APE1 on different transcription factors such as
124 NF-κB, AP-1, HIF-1 and STAT3 [18,39,40]. In particular, APX3330 increases disulfide bonds
125 involving C65 and/or C93 residues in APE1, impairing its redox activity [41]. APX3330
126 recently completed cancer phase I clinical trials with demonstrated safety, response and
127 APE1 target engagement [42,43]. Finally, Spiclomazine, Fiduxosin, and SB206553
128 molecules inhibit the interaction of APE1 with NPM1, a protein involved in rRNA biogenesis,
129 by directly binding to the N-terminal domain of APE1. We demonstrated that these inhibitors
130 alter the localization and the endonuclease activity of APE1, but not the rRNA maturation

131 [22] and induce apoptosis in different tumor cell lines [22,44]. To our knowledge, only one
132 study investigated the ability of the APE1-redox inhibitor (APX3330) to affect colon cancer
133 stem cells (CCSCs) growth *in vitro* and to enhance the effect of the chemotherapeutic agent
134 5-Fluorouracil (5-FU) in CCSCs xenograft mice [23]. Thus, the importance of exploring the
135 effect of different APE1 inhibitors in CRC models is apparent. Here, we used the well-known
136 HCT-116 colon cancer cell model, to explore the relevance of p53 upon APE1 inhibition,
137 and extended our findings using a 3D organoid cultures model derived from CRC affected
138 patients.
139 Due to the intricate mechanisms that characterize the CRC etiology, research has focused
140 on personalized precision medicine of CRC. The generation of patient-derived 3D tumor
141 organoids will greatly enhance our understanding of the disease complexity and the
142 heterogeneity in order to develop patient-specific therapies [45]. Organoids have a special
143 property to mirror the key-features of the original patient's tissue [46], representing an ideal
144 tool to develop patient-specific therapies by performing drug screenings.
145 Similarly to APE1, the well-known tumor suppressor gene *TP53* has been found altered in
146 most tumors [47]. The wild-type p53 protein is a transcription factor involving in cell cycle
147 arrest, senescence and apoptosis, besides being a key player in the DNA Damage
148 Response (DDR) to single-strand breaks (SSBs) and double-strand break (DSBs)
149 accumulation. Among all the mutated genes promoting CRC, p53 has an important role [48].
150 Indeed, loss of p53 function stimulates the development of the late stage of CRC and is
151 associated with poor prognosis [49]. p53 plays a role not only as a modulator of the cell
152 cycle to guarantee genome stability, but it is also directly involved in the activation of proteins
153 that are associated with DNA repair processes [50]. In particular, it has been demonstrated
154 that p53 prevents genomic instability through a BER gene expression regulation [51].
155 Importantly, p53 regulates DNA glycosylases (OGG1 and MUTYH) [52,53], APE1 [54,55],
156 Pol β [56] expression and acts as a transcriptional repressor of DNA polymerase δ [57].

157 However, it is unknown whether p53 is part of DDR starting from AP sites accumulation as
158 a consequence of APE1 inactivation or inhibition. The present study was aimed at
159 addressing this issue. Furthermore, data on whether APE1 inhibitors may affect cell viability
160 of colon cancer cells through p53-induced cell response are the focus of the work presented
161 here.
162

2. Materials and methods

2.1. Cell cultures. HCT-116 $p53^{+/+}$ and HCT-116 $p53^{-/-}$ (ATCC®) cells were grown in Dulbecco's modified Eagle's medium (EuroClone, Milan, Italy) supplemented with 10% fetal bovine serum (EuroClone). CH12F3$^{+/+/\Delta}$ and CH12F3$^{\Delta/\Delta/\Delta}$ cells were grown in RPMI 1640 (EuroClone) supplemented with 10% fetal bovine serum (EuroClone), 1X non Essential Amino Acids (EuroClone), 1 mM Sodium Pyruvate (EuroClone), 25 mM HEPES (EuroClone) and 50 μM β-mercaptoethanol (Promega, Madison, WI, USA). OCI-AML2 cells were grown in α-MEM (Invitrogen, Carlsbad, CA, USA) supplemented with 20% fetal bovine serum (EuroClone). HCC70 cells were grown in RPMI 1640 (EuroClone) supplemented with 10% fetal bovine serum (EuroClone). All culturing media were also supplemented with 2 mM GlutaMAX (EuroClone), 100 U/ml penicillin and 10 μg/ml streptomycin (EuroClone).

2.2. Human tissues. Colonic tissues were obtained upon surgical resection from the University Hospital Santa Maria della Misericordia of Udine. All patients were diagnosed with colorectal cancer. This study was approved by the ethical committee of University Hospital Santa Maria della Misericordia of Udine (CEUR-2017-PR-048-UNIUD) and all samples were obtained prior to informed consent.

2.3. Organoid culture. The generation of patient-derived tumor organoids was performed as described by [58] with some modifications. Tumor intestinal tissue was washed with ice-cold PBS supplemented with 100 U/ml penicillin and 10 μg/ml streptomycin (EuroClone) several times. Tumor tissue was homogenized with scissors and then digested with 0.26 U/ml Liberase (Sigma-Aldrich, St. Louis, MO, USA) in basal medium, composed of Advanced DMEM/F12 (Life Technologies, Carlsbad, CA, USA) supplemented with 2 mM Glutamax (Life Technologies), 10 mM HEPES (Life Technologies), 100 U/ml penicillin and 10 μg/ml streptomycin (EuroClone) complemented with 100 μg/ml Primocin (InvivoGen,

189 Diego, CA, USA) and 10 µM Y-27632 (Abcam, Cambridge, UK) for 1 h at 37 °C shaking at
190 250 rpm. The resulting fraction was passed through a 100-mm cell strainer. The filtered
191 solution was centrifuged at 1,200 rpm for 5 min at 4°C. The cell pellet was resuspended with
192 Red Blood Cell (RBC) Lysis Buffer (BioLegend, San Diego, CA, USA) and incubated for 10
193 min at room temperature (RT) in the dark. RBC buffer was neutralized adding basal medium
194 complemented with 10% fetal bovine serum (BioWest, Nuaillé, France). The resulting
195 solution was centrifuged at 1,200 rpm for 5 min at 4°C and the cell pellet was resuspended
196 with 3 ml of basal medium. Cells were counted with a Burker chamber and 200,000 cells/10
197 µl were mixed with 20µl of Matrigel and 30µl drop was plated in a single well of 24-well.
198 After polymerization of Matrigel (Corning®, Corning, NY, USA) for 10-15 min at 37°C, 500
199 µl of culture medium was added. Tumor organoids were cultured in basal medium containing
200 1X B27 (Life Technologies), 1.15 mM N-acetylcysteine (Sigma-Aldrich), 10 mM
201 Nicotinamide (Sigma-Aldrich), 10 nM Gastrin I (Tocris Bioscience, Bristol, UK), 10 nM
202 Prostaglandin E_2 (Sigma-Aldrich), 500 nM A83-01 (R&D System, Minneapolis, MN, USA),
203 50 ng/ml mEGF (PeproTech, London, UK), 3 µM SB202190 (Sigma-Aldrich), 10% Noggin
204 Conditioned Medium, 20% R-Spondin1 Conditioned Medium, 10 µM Y-27632 (Abcam) and
205 100 µg/ml Primocin (InvivoGen). The medium was refreshed every two/three days. Tumour
206 organoids were passaged 1:4 every one/two weeks.
207
208 **2.4. Treatments.** Compound #3 was kindly provided by the National Center for Advancing
209 Translational Sciences. APX2009 was kindly provided by Professor Mark R. Kelley (Indiana
210 University, School of Medicine). Fiduxosin, SB206553, Spiclomazine were purchased as
211 previously described [22]. All compounds were solved in dimethyl sulfoxide (DMSO). IC_{50}
212 values were calculated using Combenefit 2.021 Software.
213

2.5. RNA interference. One day before transfection, cells were seeded in 60-mm plates at a density of 600,000 cells per plate. Cells were then transiently transfected with 100 pmol siRNA APE1 5□-UACUCCAGUCGUACCAGACCU-3□or the scramble control siRNA5□-CCAUGAGGUCAUGGUCUGdTdT-3□ (Dharmacon, Lafayette, CO, USA) using DharmaFECT reagent (Dharmacon). After 72 h upon transfection, cells were collected and whole cell extracts were prepared.

2.6. Preparation of the cell extracts and protein quantification. For the preparation of whole cell lysates, 200,000 HCT-116 cells were plated on 6-well plates and, the following day, cells were treated with Compound #3 or APX2009. After 48 h cells were collected by trypsinization and centrifuged at 250 x *g* for 5 min. The supernatant was removed, and the pellet was washed once with PBS and then centrifuged again as described before. Cell pellet was resuspended in lysis buffer containing 50 mM Tris-HCl (pH 7.4), 150 mM NaCl, 1 mM EDTA, 1% w/v Triton X-100 supplemented with 1 mM protease inhibitor cocktail (Sigma-Aldrich), 1 mM DTT, 0.5 mM phenylmethylsulfonyl fluoride (PMSF), 1 mM NaF and 1 mM Na_3VO_4 for 30 min at 4 °C. After centrifugation at 13,000 rpm for 20 min at 4 °C, the supernatant was collected as a whole cell lysate. The protein concentration was determined by using Bio-Rad protein assay reagent (Bio-Rad, Hercules, CA, USA).

2.7. Antibodies and Western blotting analysis. For Western blotting analyses, whole cell lysates were prepared and 30 µg of proteins were resolved on 12% SDS–PAGE, transferred onto nitrocellulose membranes (Schleicher & Schuell Bioscience, Keene, NH, USA) and incubated with antibodies for p53 1:1000 (#sc-126, Santa Cruz Biotechnology, Dallas, TX, USA), APE1 1:1000 (#NB-100116, Thermo Fisher Scientific, Waltham, MA, USA), p21 1:1000 (#2947, Cell Signaling Technology, Danvers, MA, USA) and actin 1:2000 (#A2066, Sigma-Aldrich). The corresponding secondary antibodies labelled with IR-Dye (goat anti-

240 rabbit IgG IRDye 680 and goat anti-mouse IgG IRDye 800, LI-COR Biosciences, Lincoln,
241 NE, USA) were used (1:10,000). Blots were developed by using the NIR Fluorescence
242 technology (LI-COR Biosciences). Images were acquired and quantified by using an
243 Odyssey CLx Infrared Imaging System (LI-COR Biosciences).
244
245 **2.8. Metabolic activity.** Metabolic activity of HCT-116 cell lines was measured through the
246 MTS CellTiter 96 AQueous One Solution Cell Proliferation Assay and through RealTime-
247 Glo™ MT Cell Viability Assay (Promega) according to the manufacturer's instructions. In
248 details, 5,000 cells were plated on transparent or black 96-well plates, as needed, and the
249 day after, cells were treated with the indicated drugs for 48 h. Metabolic activity of CH12F3
250 cell lines was measured with CellTiter 96® Aqueous One Solution Cell Proliferation Assay
251 (Promega) according to the manufacturer's instructions. In details, 10,000 cells were plated
252 on black 96-well plates and the day after cells were treated with increasing amounts of
253 Compound #3 or APX2009 at the indicated concentrations for 48 h. Metabolic activity of
254 patient-derived tumor organoids was measured through the RealTime-Glo™ MT Cell
255 Viability Assay (Promega) according to the manufacturer's instructions. In this case, 3,000
256 cells derived from tumor organoids were plated together with Matrigel on black 96-well plates
257 and incubated for three days for allowing the generation of the organoids. Tumor organoids
258 were treated with increasing amounts of Compound #3 for 48 h. For metabolic assay, Y-
259 27632 was removed from the culture medium.
260
261 **2.9. AP sites measurements.** For the AP sites measurements, 200,000 HCT-116 cells
262 were plated on 6-well plates and, the following day, cells were treated with Compound #3.
263 After 48 h, genomic DNA was extracted from the collected cells using QIAamp DNA Mini Kit
264 (Qiagen, Hilden, Germany), and concentration and purity were determined by NanoDrop
265 Microvolume Spectrophotometer (Thermo Fisher Scientific). Samples of 100 μg/ml

genomic DNA were analyzed to quantify abasic sites in DNA using the DNA Damage Quantification Kit -AP Site Counting- (Dojindo Molecular Technologies, Kumamoto, Japan) according to the manufacturer's instructions.

2.10. Comet assay analysis. The comet assay was performed as previously described [59]. Specifically, 25,000 cells were plated on 24-well plates and the day after cells were treated with 0.5 μM Compound #3. After 48 h, cells were collected and mixed with low melting point agarose at 37 °C, and the mixture was applied to a agarose pre-coated glass coverslip to form a thin layer. Cold lysis buffer was added to lyse cells at 4 °C. After 1 h, the glass coverslip was moved into alkaline electrophoresis buffer for 30 min to unwind DNA. Electrophoresis was carried out at 25 V and 300 mA for 30 min. The glass coverslip was washed with neutralizing buffer for three times and stained by Sybr Gold 1X (Thermo Fisher Scientific) for 30 min in dark. Comets were recorded by laser scanning confocal microscope (LEICA TCS SP2, Leica Microsystems, Wetzlar, Germany). The tail moment was analyzed for 100 cells at random by OpenComet software.

2.11. Quantitative real-time reverse transcriptase-PCR. For RNA extraction, 200,000 HCT-116 cells were plated on 6-well plates and, the following day, were treated with Compound #3 or APX2009. After 48 h, total RNA was extracted from the collected cells using the NUCLEOSPIN RNA II (MACHEREY-NAGEL GmbH & Co., Duren, Germany). The quality of the RNA samples was tested on an agarose gel. Then, single-strand cDNA was obtained from 1 μg of purified RNA using SensiFAST cDNA Synthesis Kit (Bioline Meridian Bioscience, Cincinnati, OH, USA). qRT-PCR was performed using SensiFAST SYBR No-ROX Kit (Bioline Meridian Bioscience) and a CFX96 Real-Time System (Bio-Rad). Each sample analysis was performed in triplicate. Samples without template and without reverse transcriptase were used as negative control,. The cycling parameters contemplate a first

denaturation at 95 °C for 10 s and then 40-cycles of annealing/extension at 60 °C for 30 s. In order to verify the specificity of the amplification, a melting-curve analysis was performed, immediately after the amplification protocol. Relative gene expression was calculated with the $2^{-\Delta\Delta Ct}$ method. The sequences of the primers used are the following: APEX1 For 5'-CCTGGACTCTCTCATCAATACTGG-3', APEX1 Rev 5'-AGTCAAATTCAGCCACAATCACC-3', BIRC5 For 5□ACCGCATCTCTACATTCAAG-3□ BIRC5 Rev 5□CAAGTCTGGCTCGTTCTC-3□ DNA polδ For 5'-GCTCCGCTCCTACACGCTCAA-3', DNA polδ Rev 5'-GTCTGGTCGTTCCCATTCTGC-3' and Actin For 5□CGCCGCCAGCTCACCATG-3□ Actin Rev 5□CACGATGGAGGGGAAGACGG-3□

2.12. Caspases activity assay. The activities of caspases 3/7 were examined via a fluorescence-based assay using Apo-ONE® Homogeneous Caspase-3/7 Assay (Promega) according to the manufacturer's instructions. In details, 5,000 cells were plated on white 96-well plates and the day after cells were treated with increasing amounts of Compound #3 or APX2009 for 48 h.

2.13. Cell Mito Stress test. Analyses of the mitochondrial function of HCT-116 cells were performed by using XFe Extracellular Flux Analyzer (Seahorse, Agilent Technologies, Santa Clara, CA, USA) as previously described [60]. In details, 5,000 cells were seeded and cultured in XF Cell Culture Microplates (Agilent Technologies). Before the measurements, the culture medium was removed from each well and replaced by 500µl of Seahorse XF Base Medium (Agilent Technologies), pre-warmed at 37 °C and supplemented with 10 mM glucose (Sigma-Aldrich), 1 mM pyruvate (EuroClone), 2 mM glutamine (Sigma-Aldrich), at pH 7.4. Cells were incubated in a CO_2-free incubator at 37 °C for 1 h and OCR (oxygen consumption rate) was detected under basal conditions. The following compounds were

prepared at appropriate concentrations for each injection port to reach the final concentration of 0.5 µM oligomycin A, 0.5 µM FCCP, 1 µM rotenone and 1 µM antimycin A (Sigma-Aldrich). Volumes of respectively 56, 62, 69 and 73 µl of compounds were added to each injection port. Then, after a 3-min pause, 3 response measurements were taken between each addition. OCR values were normalized to the protein content (µg) of each well obtained by the Bradford method.

2.14. Immunofluorescence. Patient-derived tumor organoids were grown on a slide and fixed in 4% paraformaldehyde for 20 min at 37°C, then washed with PBS 1X, treated with 0.1 M glycine in PBS 1X for 10 min and permeabilized with 0.5% Triton X-100 in PBS 1X for 5 min. After washing with PBS 1X and blocking for 1 h with 1% BSA, 10% FBS, 0.5% Triton X-100 in Washing Buffer (10 mM Tris HCl pH7.4, 150 mM NaCl and 0.01% Tween 20) organoids were incubated with primary antibodies diluted in blocking solution o/n at 4°C. After several washes in PBS 1X, organoids were incubated with labeled secondary antibodies for 2 h at RT. F-actin was stained with 0.165 µM Alexa Fluor™ 594 Phalloidin (Thermo Fisher Scientific) for 20 min at RT. For nuclear staining, organoids were incubated with 14.3 mM DAPI (Thermo Fisher Scientific) for 5 min at RT. Organoids were washed and mounted with Mowiol mounting medium. The following antibodies were used: anti-Ki67 1:200 (#AB92742, Abcam), anti-OLFM4 1:200 (#14369S, Cell Signaling Technology), anti-E-Cadherin 1:50 (#610404, BD Biosciences, San Jose, CA, USA) and anti-Lysozyme 1:200 (#A009902-2, Agilent Technologies). For detection, Alexa Fluor-488 (#711-546-152 and #715-546-150 Jackson ImmunoResearch, Ely, UK) antibodies were used. Fluorescent images were collected using a laser scanning confocal microscope (LEICA TCS SP8, Leica Microsystems). Brightfield images were collected using a microscope (LEICA MC170 HD, Leica Microsystems).

2.15. Library preparation and next-generation sequencing. Genomic DNA from tumor organoid was extracted using the QIAamp DNA Mini Kit (Qiagen) and quantified by using the Quant-iT™ PicoGreen™ dsDNA Assay Kit (LifeTechnologies). Briefly, barcoded libraries were generated from 50 ng of DNA per sample (N=3) using the Ion AmpliSeq Library Kit Plus (Thermo Fisher Scientific) and two premixed pools of 952 primer pairs (Thermo Fisher Scientific), according to manufacturer's instructions. Clonal amplification of libraries was performed by emulsion PCR on an Ion Chef Instrument. The prepared libraries were then sequenced on an Ion S5 GeneStudio Sequencer using a Ion 530 Chip and the Ion 510/520/530 kit–Chef (all Thermo Fisher Scientific).

2.16. Data analysis and Variant prioritization. We analyzed data using Variant Caller v5.10 (Thermo Fisher Scientific). Variant caller format files were annotated with Ion Reporter 5.10 (Thermo Fisher Scientific) and wANNOVAR. Somatic variants were called when a position was covered at least 100X. We set the clinical sensitivity of point mutations and indels at 5%. Variant prioritization for *TP53* was based on population frequency, quality values and functional consequences. Synonymous variants were excluded. Variants were filtered based on their frequency ExAC datasets (http://exac.broadinstitute.org) and on clinical associations (ClinVar database) (https://www.ncbi.nlm.nih.gov/clinvar).

2.17. Bioinformatics analysis. Analysis of *APEX1* gene expression in colon cancer was performed through TCGA data retrieval from cbioportal and CMS class information were accessed from the original Consensus Molecular Stratification of colon cancer. Differential gene expression analysis was conducted by Mann Whitney test. APE1 interactors analysis in colon cancer was performed using the differential gene expression results from TCGA and normal datasets (GTEX data) for the genes encoding the interacting partners of APE1 for colon cancer (COAD). Data was obtained via the GDC data portal hub

370 (https://portal.gdc.cancer.gov/, last accessed July 2018). The RUVSeq package inside the
371 R/Bioconductor environment was used to eliminate the batch effect coming from the
372 combination of two data sources [61]. In order to better estimate the differentially expressed
373 genes between the tumor and the normal corresponding datasets, we obtained “in-silico
374 empirical” negative controls, i.e., the least significantly DE genes based on a first-pass DE
375 analysis performed prior to RUVg normalization [61]. Differentially expressed genes
376 (multiple correction adjustment using the Benjamini-Hochberg method, $p<0.05$; absolute log
377 fold changedifference≥1) were used to perform enrichment and survival analyses.
378 Enrichment analysis of the DE genes was performed using the DAVID functional annotation
379 tool based on GO biological process and cellular component terms [62]. For the survival
380 analysis, Kaplan-Meier plots were drawn using the RTCGA Bioconductor package [63],
381 which uses maximally selected rank statistics (maxstat) to determine the optimal cutpoint
382 for continuous variables. Division of the samples was done within the 30-70% percentile
383 range of gene expression by the optimal cutpoint value. The Benjamini-Hochberg method
384 was used for p-value correction of Kaplan-Meier plots.
385
386 **2.18. Statistical analyses.** All reported values are represented as the mean ± SD or mean
387 ± SEM of at least three biological replicates. Statistical analyses were performed using the
388 Student’s t-test. $P<0.05$ was considered as statistically significant.
389

3. Results

3.1. APE1 is overexpressed in colorectal cancer and the inhibition of its endonuclease activity triggers p53-mediated effects on cell metabolism

APE1 overexpression is correlated with tumor progression of many cancers, but little information is available on colorectal cancer (CRC) [23,24,64]. In order to further determine the involvement of APE1 in CRC, we took advantage of the information available from TCGA data sets of CRC. By performing differential gene expression (DEG) analysis on the TCGA COAD RNA-seq V2 data, we compared the expression profile of the four consensus molecular subtypes (CMS) of CRC versus normal control samples [PMC4636487]. The DEG was computed by the non-parametric Mann Whitney test. A significant upregulation of the *APEX1* gene in the four CMS classes was identified compared to the normal one (Fig. 1A) (p-value=$1.7e^{-15}$, $4e^{-11}$, $7.2e^{-14}$, $3.5e^{-11}$, for the CMS class 1-4, respectively), however there was no significant difference between the CMS classes analysed. These data demonstrate that APE1 is generally overexpressed in CRC, supporting the hypothesis that it could represent a novel target for the treatment of this cancer type.

We analyzed the effects of APE1 inhibition on colon cancer cell lines using a number of APE1 specific small molecule inhibitors: Compound #3, which blocks APE1-endonuclease activity thus leading to genome instability [35]; APX2009, which inhibits APE1-redox function, leading to cell-cycle arrest and apoptosis in different cancer cell models [38], and Fiduxosin, SB206553 and Spiclomazine, as inhibitors of the well-known interaction between APE1 and NPM1, leading to an alteration of the APE1-endonuclease activity and to apoptosis in different tumor cell lines [22,44]. A schematic representation of the APE1-inhibitors used in this study is shown in Fig. 1B.

To determine the p53 contribution in APE1 inhibitors induced effects, we took advantage of the well-known HCT-116 $p53^{+/+}$ and HCT-116 $p53^{-/-}$ isogenic colon cancer cell lines, which are wild-type and knock-out for p53 gene expression, respectively [65] (Fig. 1C, top left

panel). Experimentally, HCT-116 cells were treated with increasing concentrations of different APE1 inhibitors for 48 hours. The metabolic activity of viable cells was measured by using the MTS assay, a colorimetric assay which measures the reduction of MTS tetrazolium compound into formazan in mitochondrial metabolically active cells. The treatment with the APE1-endonuclease inhibitor Compound #3 demonstrated that HCT-116 $p53^{+/+}$ cell line was significantly more sensitive, at the doses of 0.25 μM and 0.5 μM, than HCT-116 $p53^{-/-}$ (Fig. 1C, top in the middle panel and Table 1 for IC_{50} values). In order to understand if the inhibition of APE1-redox activity could have some effects on HCT-116 cell lines, we treated cells with the APX2009 compound. We did not find a significant difference between HCT-116 $p53^{+/+}$ and HCT-116 $p53^{-/-}$ cell metabolism upon APX2009 treatment, even if a mild effect can be observed (Fig. 1C, top right panel and Table 1 for IC_{50} values). Similarly, no significant differences, between the two cell lines, were found when inhibitors of APE1 and NPM1 interaction were used, with Fiduxosin being the most toxic for both cell lines (Fig. 1C, bottom panel and Table 1 for IC_{50} values). These findings were in agreement with the presence of no significant difference in the expression levels of both APE1 and NPM1, as measured at the mRNA and protein levels (Fig. S1A, B). Moreover, to further confirm the differential effect of Compound #3 and APX2009 on cell metabolism of HCT-116 $p53^{+/+}$ and HCT-116 $p53^{-/-}$ cell lines, we performed a luminescence-based metabolic assay (RealTime-Glo). Compared to MTS assay, previously used, RealTime-Glo is a more sensitive assay based on the measurement of the reducing potential of mitochondrial metabolic active cells, considering the luminescent signal produced from the reduction of the substrate used by the luciferase, and thus mitochondrial metabolism. RealTime-Glo assay demonstrated that HCT-116 $p53^{+/+}$ cells presented an impairment of metabolic activity in comparison to HCT-116 $p53^{-/-}$ upon Compound #3 treatment, especially at the dose of 0.5 μM, confirming the data previously obtained through MTS assay (Figure 1D, right panel and Table 1 for IC_{50} values). Interestingly, RealTime-Glo assay revealed that HCT-116 $p53^{-/-}$

442 cells underwent a major loss of metabolic activity compared to HCT-116 $p53^{+/+}$ cells upon
443 APX2009 administration in a dose-dependent manner, particularly at the doses of 2.5 μM
444 and 5 μM (Fig. 1D, right panel and Table 1 for IC_{50} values). These data demonstrated that
445 the small difference in metabolic activity that we observed with MTS assay (Fig 1C, top right
446 panel) was much more apparent when the more sensitive RealTime-Glo assay was used.
447 in place of the MTS assay. In order to exclude that the toxic effect could be associated with
448 an alteration of the doubling time of the HCT-116 $p53^{+/+}$ and $p53^{-/-}$ cell lines, we calculated
449 it (HCT-116 $p53^{+/+}$ 38±2.2 h, HCT-116 $p53^{-/-}$35 ±2.4 h)and no difference was observed. This
450 excludes an alteration of the proliferation index as the cause of the effects on cell viability
451 between the two cell lines.
452 In order to further validate the specificity of Compound #3 and APX2009 as APE1 inhibitors
453 in the range of doses used in the present study, we took advantages of $CH12F3^{+/+/\Delta}$ and
454 $CH12F3^{\Delta/\Delta/\Delta}$ cell lines [66], a recently developed murine cell model containing two and zero
455 copies of *APEX1* alleles, respectively (Fig. 1E, left panel). Both CH12F3 cell lines were
456 treated with increasing concentrations of Compound #3 or APX2009 for 48 hours and then,
457 the cellular metabolism of viable cells was measured by using a luminescence-based assay
458 (CellTiter-Glo), which evaluates the amount of total ATP produced by cells. As shown in Fig.
459 1E, APE1-endonuclease and -redox inhibitors specifically affect $CH12F3^{+/+/\Delta}$ but not
460 $CH12F3^{\Delta/\Delta/\Delta}$ cell line, as expected, confirming the high specificity of the inhibitors, under the
461 experimental conditions used (Table 1 for IC_{50} values). In the case of the effects of
462 Fiduxosin, SB206553 and Spiclomazine, their specificity was previously demonstrated by
463 us [22,44].
464 In conclusion, data obtained indicate that the sensitivity of HCT-116 cells to Compound #3
465 and APX2009 treatment was dependent on their p53 status. Moreover, the inhibition of
466 APE1-NPM1 interaction impairs cell metabolism independently of p53 status. Interestingly,

while the toxic effect of Compound #3 was dependent on the expression of p53, a more toxic effect of APX2009 was apparent in p53 knock-out cells.

3.2. Inhibition of APE1-endonuclease activity promotes p53 activation

We then evaluated whether APE1 inhibition could promote p53 activation. We focused only on Compound #3 and APX2009, since the APE1-NPM1 inhibitors did not display any significant difference in terms of biological effects exerted on HCT-116 cell lines. p53 activation is part of DDR triggered by single-strand breaks (SSBs) and double-strand breaks (DSBs) formation. We determined whether the amount of AP sites and SSBs could be affected by the treatment with Compound #3 in HCT-116 cell lines. AP sites measurements (Fig 2A) and comet assay analyses (Fig. 2B and C) clearly demonstrated that Compound #3 treatment promoted a significant increase of AP sites and SSBs formation in both HCT-116 $p53^{+/+}$ and HCT-116 $p53^{-/-}$ cell lines independently of the p53 status at both the doses tested (0.5 μM and 3 μM). The non-significant difference in the levels of AP sites and SSBs between both HCT-116 cell lines is in agreement with the non-differential expression of APE1 between the two cell lines used (Fig. S1).

In order to get a better understanding of the relationship existing between p53, its gene target genes and the inhibition of APE1 enzymatic activity in HCT-116 cell lines, we analyzed the protein and mRNA expression levels of p53 and those of some p53-target genes upon Compound #3 treatment. In details, HCT-116 $p53^{+/+}$ and HCT-116 $p53^{-/-}$ cells were treated with increasing concentrations of Compound #3 (0.25 μM and 0.5 μM) and cells were collected and tested 48 hours later. These doses, with limited effects on cell viability, allowed to avoide epiphenomena due to general toxic effects and allowed comparison to data obtained with those obtained with the redox-inhibitor (see below). Upon the administration of Compound #3, we analyzed the protein levels of APE1, p53, and p21, one of the major downstream targets of p53 [47], through Western blotting. We observed a significant

493 increase of p53 and p21 protein levels upon Compound #3 administration in HCT-116 $p53^{+/+}$
494 cells only, indicating a p53 activation possibly due as a consequence of cell DDR induction
495 (Fig. 2D). Moreover, the inhibition of APE1-endonuclease activity did not considerably alter
496 neither APE1 nor NPM1 protein levels in both cell lines, exerting only slight effects.
497 Densitometric analysis of p53, p21, APE1, and NPM1 protein levels, normalized to actin
498 levels, is shown in Fig. 2E. Moreover, to further confirm the unaltered levels of APE1 gene
499 expression upon Compound #3 treatment, we analyzed its mRNA expression. No
500 statistically significant changes in APE1 transcript were observed (Fig. S1C), confirming that
501 the higher sensitivity of HCT-116 $p53^{+/+}$ cell line to Compound #3 is not due to an impairment
502 of APE1 expression. Furthermore, to test a possible impact of the activation of the p53
503 pathway on another known p53-target gene, negatively regulated by p53 and involved in
504 BER [11,57,67–69], we analyzed the mRNA expression level of DNA Polymerase δ (DNA
505 Polδ). As it is shown in Fig. 2F, the level of transcripts of DNA Polδ decreased upon
506 Compound #3 treatment in HCT-116 $p53^{+/+}$ cells only, in line with p53 induction. These data
507 support the hypothesis that APE1-endonuclease inhibition causes the functional activation
508 of p53 protein acting both as a transcriptional activator and repressor of different target
509 genes.
510 In order to further support that APE1 inhibition may result in p53 activation, a knockdown
511 approach, through specific siRNA targeting APE1, was used. As shown in Fig 2G, knock
512 down of APE1 promoted an increased expression of p53 in HCT-116 $p53^{+/+}$ cell line,
513 demonstrating a mutual inverse relationship between APE1 and p53 (Fig. 2G). Finally, to
514 generalize the stimulatory effect by Compound #3 on p53 expression, we treated two
515 additional tumor cell lines, i.e. AML2 as a model of acute myeloid leukemia cells [70] and
516 HCC70 cell line, a triple negative breast cancer cell line [71]. These cell lines harbor a wild-
517 type form [70] and a missense mutation (p.R248Q) [71] of the *TP53* gene, respectively.
518 *TP53* p.R248Q is a gain-of-function mutation that causes an aberrant overexpression of the

519 p53 protein. AML2 and HCC70 cell lines showed an increased expression of p53 upon
520 Compound #3 treatment, demonstrating that the activation of p53 upon inhibition of APE1-
521 endonuclease activity could be a generalized phenomenon across different cancer cell lines
522 (Fig. 2H and I) and not only colon specific. Altogether, these data confirm that APE1-
523 endonuclease inhibitor treatment of different cancer cell lines promotes p53 expression and
524 its functional induction.
525 DNA damage activating the p53-p21 pathway may lead to cell apoptosis through caspase
526 activation [47]. Therefore, we performed a caspase activity assay to measure apoptosis
527 induction by Compound #3 treatment (Fig 2L). After 48 hours of treatment with increasing
528 concentrations of Compound #3, Apo-ONE assay was used to quantify relative levels of
529 apoptosis. The treatment with APE1 inhibitor induced the activation of the caspase pathway
530 in both colon cancer cell lines (Fig. 2L) occurring only at the highest dose (3 μM) of
531 treatment. However, no differences were apparent between the two cell lines, confirming
532 that Caspase activation was independent of p53-activation and was present only at highest
533 dose of treatment with Compound #3. Data not shown also demonstrated that Compound
534 #3-treatment did not exert any significant differential effect on cell cycle of the two isogenic
535 HCT-116 cell lines.
536 These experiments, coupled with the metabolic assays, indicate that the inhibition of the
537 APE1-endonuclease activity promoted a p53-induced response involving mitochondria,
538 which may explain the higher susceptibility of $p53^{+/+}$ cell metabolism to Compound #3
539 treatment in the absence of significant Caspase-3 activation and of differential effects on
540 cell cycle between the two HCT-116 isogenic cell lines.
541
542 **3.3 Inhibition of APE1-redox activity does not affect p53 expression**
543 We analyzed whether inhibition of APE1-redox activity could affect p53 expression. We
544 checked the efficacy of APX2009 treatment on HCT-116 colon cancer cell lines,

qRT-PCR on the baculoviral inhibitor of apoptosis repeat-containing 5 (BIRC5), also known as Survivin, that was already demonstrated to be a target of APE1-redox function [40]. Treatment with increasing concentrations of APX2009 (Fig. 3A) promoted a decrease in the expression levels of BIRC5 transcript in both HCT-116 cell lines (Fig. 3A), in line with previously demonstrated data on different cell lines [40].

To assess whether APE1-redox inhibitor stimulates the p53-pathway, we performed the same set of experiments, as with Compound #3, but with APX2009. We used APX2009 at concentrations of 5 μM and 10 μM, that promoted a reduction in cell viability of less than 40% similar to the conditions used with Compound #3 treatment. As shown in Fig. 3B and C, no differences in p53 and in the expression of the p21 target gene were observed upon the administration of the redox inhibitor. Moreover, DNA Polδ transcript did not significantly change following APX2009 administration, in agreement with the lack of any stimulatory effects by the APE1-redox inhibition on p53 levels (Fig. 3D). Moreover, the caspase activity assay demonstrated a dose-dependent activation of the caspase pathway indistinctly in both colon cancer cell lines (Fig. 3E).

Taken together, these experiments demonstrate that the inhibition of the APE1-redox activity does not activate a p53-mediated cell response and this is in agreement with data on cell metabolism.

3.4 Inhibition of APE1-endonuclease activity impairs mitochondrial activity in a p53-dependent manner

Data obtained so far, through MTS and RealTime-Glo analyses, point to a major role of the p53-dependent effect of Compound #3 on cell viability due to metabolic effects associated with mitochondrial toxicity. In order to better characterize this aspect, we directly analyzed mitochondrial activity using the Cell Mito Stress Test [72] upon Compound #3 treatment. Specifically, HCT-116 $p53^{+/+}$ and HCT-116 $p53^{-/-}$ cell lines were treated with 0.5 μM of

571 Compound #3 for 48 hours and were analysed for mitochondrial respiration. The parameters
572 of basal oxygen consumption, respiration coupled to ATP production, spare respiratory
573 capacity and maximal respiration were obtained through oxygen consumption rate (OCR)
574 profile. As represented in Fig. 4A, OCR profile indicates that Compound #3 impaired the
575 mitochondrial activity of HCT-116 $p53^{+/+}$ cells, while the treatment did not significantly alter
576 the mitochondrial function of HCT-116 $p53^{-/-}$ cells. In particular, the OCR values were
577 comparable between the two colon cancer cell lines under basal conditions. Interestingly,
578 Compound #3 treatment affected the majority of the respiratory parameters in a p53-
579 dependent manner (Fig. 4B). Among them, the basal and ATP-coupled respiration was
580 significantly lower in HCT-116 $p53^{+/+}$ than the isogenic $p53^{-/-}$ counterpart upon treatment.
581 Moreover, the spare respiratory capacity and maximal respiration were impaired in HCT-
582 116 $p53^{+/+}$ treated cells in comparison to the untreated condition. On the other hand, we did
583 not observe any difference in mitochondrial function in p53-null colon cancer cell line upon
584 treatment. The OCR profiles of HCT-116 $p53^{+/+}$ and $p53^{-/-}$ cell lines with Compound #3 at
585 different concentrations (0.25 μM and 1 μM) are shown in Fig. S2, confirming the obtained
586 results, particularly at the dose of 1 μM.
587 Overall, the data obtained suggest that the expression of p53 is responsible for the observed
588 effects on cell metabolism, upon inhibition of APE1-endonuclease activity, through an
589 involvement of mitochondrial respiratory function.
590

591 **3.5 Inhibition of APE1-endonuclease activity sensitizes p53 expressing cell lines to**
592 **MMS treatment**

593 Based on the results obtained so far, we analyzed the effect of p53 on cell metabolism in
594 combination with a genotoxic insult, which is specifically repaired through the enzymatic
595 activity of APE1 and BER [73]. We used methyl methanesulfonate (MMS), an alkylating
596 agent generating damages specifically repaired through BER [73]. Experimentally, HCT-116

597 cells were treated with increasing concentrations of Compound #3 (0.25 μM and 0.5 μM) for
598 40 hours and in combination with MMS (range from 200 μM to 600 μM) for additional 8 hours
599 (Fig. 5). After a total of 48 hours of treatment, cell metabolism was measured using the MTS
600 assay (Table 1 for IC_{50} values). The graphs in Fig. 5A-C clearly shows that the two isogenic
601 cell lines responded similarly sensitive to MMS. Interestingly, when Compound #3 was used
602 in combination with MMS, the sensitivity to the drug treatment increased (Fig. 5A-C);
603 however, the p53-null colon cancer cells were significantly less sensitive to combination
604 treatment than the isogenic counterpart (Table 1 for IC_{50} values), in particular at the dose of
605 600 μM of MMS, in agreement with the stimulatory effect of Compound #3 on p53 expression
606 demonstrated above.
607 These results suggest that p53-status is essential for cellular resistance to genotoxic stress
608 upon the inhibition of APE1-endonuclease activity.
609
610 **3.6 Inhibition of APE1-endonuclease activity exerts toxic effects on patient-derived**
611 **tumor organoids metabolism and is associated with the p53-mutational status**
612 In order to further validate the possible opportunity of targeting the APE1-endonuclease
613 activity in CRC and further supporting our data previously obtained with HCT-116 isogenic
614 cancer cell lines, we performed targeted experiments by using 3D tumor organoids derived
615 from three different patients affected by colon cancer (P12, P14 and P16). The molecular
616 and morphological characterization, obtained through immunofluorescence, is shown in Fig.
617 6A. Patient-derived tumor organoids were positive for the most common intestinal markers,
618 such as Ki67 (proliferating cells), OLFM4 (intestinal stem cells), E-Cadherin (intestinal
619 epithelial cells) and Lysozyme (Paneth cells). Representative images of the molecular
620 morphology of the patient-derived tumor organoids are shown in Fig. 6B. To check the p53-
621 functional status of these model organoids, genomic DNA was isolated from tumor
622 organoids and used as a template for next generation sequencing analysis, using the

623 Torrent S5 GeneStudio NGS platform. After variant calling filtration and annotation, we
624 detected a c.586C>T stop-gain mutation (p.R196X) in P14 and a c.524G>A missense
625 mutation (p.R175H) in P16, the latter being a structural aminoacidic substitution causing a
626 *TP53* gain-of-function and wild-type alleles in P12 (Fig. 6C). All samples did not bear any
627 pathogenic alteration of *APEX1* gene sequence. The western blotting analysis
628 demonstrated that p53 was expressed in P12 and P16 but not in P14, in agreement with
629 sequencing data (Fig. 6D). No major differences in APE1 protein expression level were
630 assessed among tumor organoids (Fig. 6E), with only a mild increase in P14 and P16 with
631 respect to P12. We treated the different tumor organoids with increasing concentrations of
632 Compound #3 (range from 0.5 to 5 μM) and cell metabolism was measured by using
633 RealTime-Glo assay upon 48 hours of treatment. Interestingly, the treatment with APE1-
634 endonuclease inhibitor impaired the cell metabolism of all tumor organoids in a dose-
635 dependent manner but to different extents (Fig. 6F and Table 1 for IC_{50} values). The
636 reduction of cell metabolism was observed within a range of 40-65% at the concentration of
637 5 μM. Interestingly, we observed a different cytotoxic sensitivity of the three tumor organoids
638 to Compound #3 that was dependent on their p53 status. In particular, tumor organoids
639 expressing wild-type p53 (P12) and the R175H gain-of-function mutant (P16) were more
640 sensitive to APE1 inhibition than the P14 null-mutant, in agreement with the data obtained
641 with the colon cancer cell lines.
642 Even though the limited number of sample patients, these results indicate that the inhibition
643 of APE1-endonuclease activity significantly hampers the patients-derived tumor organoids
644 metabolism and is associated with the p53 mutational status, in agreement with data
645 obtained with HCT-116 cell lines.
646

4. Discussion

Human cells are constantly subjected to potentially damaging events to the stability of nucleic acid, with tens of thousands of DNA lesions occurring per day [74]. The intestinal tract is exposed to multiple insults coming from metabolic activity of the microenvironment [75] and from the diet [7], that can lead to mutations or deletions in the DNA of epithelial cells. In the intestinal tract, the involvement of the direct reversal of DNA damage by O^6-methylguanine-DNA methyltransferase (MGMT), nucleotide excision repair (NER) and base excision repair (BER) have been described [7]. Alterations of these repair mechanisms are clearly associated with tumor development but also represent an emerging 'Achilles' heel' for the development of new anticancer strategies [76]. Indeed, a dysregulation of BER has been observed in different tumors, such as breast, liver, melanoma, bladder and colorectal cancer (CRC) [6,77–81]. In the case of CRC, an increased expression of BER enzymes is associated with a poor prognosis and contributes to chemoresistance [6]. In particular, higher levels of N-methylpurine-DNA glycosylase (MPG), 8-oxoguanine-DNA glycosylase (OGG1), APE1, PARP1, DNA polymerase β (Polβ) and XRCC1 are associated with adverse outcomes in patients with sporadic CRC [6,81]. Interestingly, the tumor suppressor p53, frequently mutated in the late stages of CRC [48], is involved in the regulation of DNA glycosylases (OGG1 and MUTYH) [52,53], APE1 [54,55], Pol β [56] and Pol δ [57] expression. Generally, upon genotoxic lesions, p53 regulates the expression of DNA repair genes [68], as in the case of APE1 that is negatively regulated by p53 through modulation of Sp1 stability [57]. Therefore, impaired p53 results in a loss of transcriptional regulation thus leading to BER imbalance and genome instability. Moreover, the DNA repair capacity of BER has been taken into account as a prognostic factor to 5-Fluorouracil (5-FU) treatment in CRC-affected patients, as demonstrated by a recent publication showing that a good therapy response is correlated with an observed higher activity of BER in non-malignant adjacent mucosa and a lower BER activity in tumor tissue [82]. To date, the

673 effect of the only APE1-redox inhibitor has been highlighted in different cancer cell lines. For
674 example, APX3330 inhibits cell growth in tumor endothelium/endothelial progenitor cells
675 [83], leukemia [31], pancreatic [84,85], breast [86], hepatocellular [87], prostate cancer cells
676 [88] and colon [23]. It should be noted that APE1-redox inhibitor APX3330 recently
677 completed a cancer Phase I clinical trial (https://clinicaltrials.gov/ct2/show/NCT03375086)
678 [42,43]. Thus, discovering new drugs able to inhibit the activity of APE1 in a CRC context
679 could be a promising field in the precision medicine. However, no studies targeting the
680 APE1-endonuclease activity and its effect on p53 activation have been published. Here, we
681 demonstrated the anticancer effects of different APE1 inhibitors in colon cancer cells and
682 their relationship with p53 activation. By using different technical approaches, we observed
683 a p53-dependent metabolic impairment, impacting on mitochondrial respiratory
684 mechanisms, of HCT-116 cell lines upon treatment with APE1-endonuclease inhibitor,
685 proving the effectiveness of the treatments also in a CRC context. It is noteworthy to mention
686 that the APX2009 redox inhibitor resulted more toxic to p53 knock-out cells than wild-type
687 counterpart. This observation will need additional studies to understand the molecular basis
688 for this effect.
689 In our case, the increased p53 level, following the DNA damage (AP site accumulation and
690 SSBs generation) caused by APE1-endonuclease inhibition, was not associated with any
691 changes in APE1 mRNA and protein levels, in contrast to what was previously demonstrated
692 in other papers, in which p53 was demonstrated to negatively regulate APE1 gene
693 expression [55]. Moreover, we did not observe any p53 stimulation caused by APX2009
694 treatment, therefore suggesting the possibility to target different APE1 activities by acting
695 through different response mechanisms either involving the DNA-repair or the redox-
696 functions. We also observed that the inhibition of APE1-endonuclease activity promotes p53
697 activation not only in colon cancer cells, but also in breast and leukemia cancer cell lines,
698 suggesting that the APE1 inactivation and the consequent accumulation of DNA damage

converge toward p53 activation. Thus, the use of APE1-endonuclease inhibitors could be particularly relevant considering the p53-functional status of the specific tumor.

Another relevant finding regards the effect of APE1-endonuclease inhibitor on CRC patient-derived tumor organoids. Our study demonstrates that Compound #3 impairs the viability of CRC patient-derived organoids in a dose-dependent manner and in a p53-dependent mutational status, which is in agreement with our findings obtained from cancer cell lines.

To our knowledge, the observation that the APE1-endonuclease inhibitor effects are possibly related to the p53 role on mitochondrial metabolism is extremely important. Besides cell cycle arrest, apoptosis and senescence, p53 plays an important function also in mitochondrial respiration [89]. As a regulator, p53 induces the expression of cytochrome c oxidase 2 (SCO2), ferredoxin reductase (FDXR) and glutamine 2 (GLS2), thus modulating oxidative phosphorylation and tricarboxylic acid (TCA) cycle [89,90]. Moreover, the involvement of BER in mitochondrial homeostasis has been extensively demonstrated. Indeed, p53 regulates mitochondrial BER in removing oxidized bases of the mtDNA generated by reactive oxygen species (ROS) metabolism [91]. Notably, Compound #3 sensitizes p53-expressing colon cancer cells to genotoxic treatment, such as MMS. Due to the relevance of APE1 inhibition on mitochondrial functionality in a p53-dependent manner, we performed additional bioinformatics analyses that clearly pointed to a major role of mitochondrial toxicity correlated with APE1 functional dysregulation in tumors. It is also possible that the effect of Compound #3 could be also exerted through inhibition of mitochondrial APE1 [92–94], whose role is still debated. An important confirmation of the mitochondrial role of APE1 linking to p53 activation is also supported by our recent findings (Ayyildiz D. *et al.*, submitted). In fact, when characterizing the APE1 protein-protein interactome (PPI) in different cancers cells, we found that the differential expression status of APE1 PPI was clearly associated with bad prognosis signatures in cancers (Ayyildiz D. *et al.*, submitted). TCGA analyses demonstrated that in CRC, 79% (n=287) of APE1

725 resulted in upregulation, while 21% (n=77) of the genes altered in expression were
726 downregulated (Fig. 7A). Based on the relationship existing between these differentially
727 expressed interactors, by focusing on their subcellular localizations through functional
728 enrichment analysis based on GO CC terms, we observed that 24% (n=70) of the
729 upregulated and 12% (n=9) of the downregulated interactors were mitochondria-associated
730 proteins (Fig. 7A). The subcellular localizations and enrichment results of these
731 differentially-regulated physical-interactors of APE1 are shown in Fig. 7B. The enrichment
732 analysis highlighted pathways that can improve our understanding of the importance of
733 APE1 for mitochondrial activity. Among them, mitochondrial RNA processing, fatty-acid
734 oxidation, respiratory complex III and apoptosis represented the most important ones (Fig.
735 7B). All these processes are essential for cancer metabolism [95,96], as in the case of the
736 mitochondrial respiratory complex III, that plays a role in CRC progression [97]. Interestingly,
737 some of these interactors were found to be significantly regulated in our previously published
738 microarray data [98], such as AK2, CKB, CLIC4, DNAJA1, DUT, HSPA1A, IDH1, KYNU,
739 MTCH2, SHMT2, SIRT1 and YWHAH (marked in red circle in Fig. 7B). SIRT1, which
740 regulates BER modulating the acetylation status of APE1 [73], has been found upregulated
741 in various cancer cell lines, including HCT-116 cell line [99]. The survival signature of the 79
742 interactors were also confirmed by Kaplan-Meier analysis in TCGA colon cancer dataset
743 (COAD) and BCAP31, CDKN2A, DUT, NIF3L1 and SHMT2 were associated to poor
744 prognosis (marked with red star in Fig. 7B). Together, this evidences support our findings,
745 namely the mitochondrial impairment related to p53 upon Compound #3 treatment. The
746 experimental data we provide, together with these bioinformatics analyses, support the
747 hypothesis to target mitochondrial function in cancer cells through APE1-endonuclease
748 inhibitors. More tailored studies are needed along these lines.
749 In conclusion, our data highlights novel relevant aspects regarding developing new
750 strategies for targeting BER, and especially APE1 functions, in CRC. Therefore, the

751 opportunity to use APE1-endonuclease inhibitors, such as Compound #3, in cancer therapy
752 should not be underestimated. Finally, greater treatment efficacy and reduced drug
753 resistance onset mechanisms have been demonstrated when different anti-cancer drugs
754 are combined together [100], thus the possibility of studying the effects of the different
755 combination of APE1 inhibitors with well-known chemotherapeutic agents may open new
756 perspectives in cancer biology research.
757

Conflict of interest

Mark R. Kelley is Chief Scientific Officer of Apexian Pharmaceuticals, the biotech company that has licensed APX2009 used in these studies. Apexian Pharmaceuticals had neither control nor oversight of the studies, interpretation, or presentation of the data in this manuscript. They did not have to approve the manuscript in any way prior to its submission. The content is solely the responsibility of the authors and does not necessarily represent the official views of the National Institutes of Health.

Acknowledgments

We thank all the members of the GT lab for thought-provoking discussions. We acknowledge David Maloney and Anton Simeonov (National Center for Advancing Translational Sciences) for providing Compound #3. We thank Prof. Calvin Kuo (Stanford University) for providing Rspo1 producer cells and Prof. Jeroen den Hertog (Hubrecht Institute) for providing Noggin producer cells.

Funding

This work was supported by grants from the Associazione Italiana per la Ricerca sul Cancro (IG19862) and from the European Union, European Regional Development Fund and Interreg V-A Italia-Austria 2014-2020 ITAT1096-P (Program PRECANMED ITAT1009 CUP G22F16000890006) to G.T.. M.R.K. was supported by NIH RO1 CA205166, NIH R01 CA231267, NIH R01 CA167291, NIH R01 CA167291-06S1 and NIH R01HL140961.

Authors' contributions

M.Cod. planned and carried out the experiments, performed the analysis, designed the figures and wrote the manuscript. M.Com. planned and carried out the Cell Mito Stress experiments, providing experimental interpretation of the results obtained. M.C.M helped

784 with Comet assay and AP site experiments, providing experimental interpretation of the
785 results obtained. C.M. performed NGS and data analysis. D.A. and C.Z. performed
786 bioinformatics analysis. M.R.K. provided APX2009 compound, contributed to the
787 interpretation of the results and to the writing and editing of the manuscript. G.Ter. provided
788 CRC tissue samples. C.E.P. contributed to the interpretation of the results and to the writing
789 and editing of the manuscript. G.Tel. designed the overall research plan and contributed to
790 its implementation, to the analysis of the results and to the writing and editing of the
791 manuscript.
792

References

[1] E.J. Kuipers, W.M. Grady, D. Lieberman, T. Seufferlein, J.J. Sung, P.G. Boelens, C.J.H. van de Velde, T. Watanabe, Colorectal cancer., Nat. Rev. Dis. Prim. 1 (2015) 15065. doi:10.1038/nrdp.2015.65.

[2] B. Vogelstein, E.R. Fearon, S.R. Hamilton, S.E. Kern, A.C. Preisinger, M. Leppert, A.M.M. Smits, J.L. Bos, A.M. Smits, J.L. Bos, Genetic Alterations during Colorectal-Tumor Development, N. Engl. J. Med. 319 (1988) 525–532. doi:10.1056/NEJM198809013190901.

[3] G. Smith, F.A. Carey, J. Beattie, M.J. V. Wilkie, T.J. Lightfoot, J. Coxhead, R.C. Garner, R.J.C. Steele, C.R. Wolf, Mutations in APC, Kirsten-ras, and p53--alternative genetic pathways to colorectal cancer, Proc. Natl. Acad. Sci. 99 (2002) 9433–9438. doi:10.1073/pnas.122612899.

[4] M. De Rosa, U. Pace, D. Rega, V. Costabile, F. Duraturo, P. Izzo, P. Delrio, Genetics, diagnosis and management of colorectal cancer (Review)., Oncol. Rep. 34 (2015) 1087–96. doi:10.3892/or.2015.4108.

[5] K. Tariq, K. Ghias, Colorectal cancer carcinogenesis: a review of mechanisms., Cancer Biol. Med. 13 (2016) 120–35. doi:10.28092/j.issn.2095-3941.2015.0103.

[6] N.M. Leguisamo, H.C. Gloria, A.N. Kalil, T. V. Martins, D.B. Azambuja, L.B. Meira, J. Saffi, N.M. Leguisamo, H.C. Gloria, A.N. Kalil, T. V. Martins, D.B. Azambuja, L.B. Meira, J. Saffi, Base excision repair imbalance in colorectal cancer has prognostic value and modulates response to chemotherapy, Oncotarget. 8 (2017) 54199–54214. doi:10.18632/oncotarget.14909.

[7] J. Fahrer, B. Kaina, Impact of DNA repair on the dose-response of colorectal cancer formation induced by dietary carcinogens., Food Chem. Toxicol. 106 (2017) 583–594. doi:10.1016/j.fct.2016.09.029.

[8] A.M. Alhadheq, J. Purusottapatnam Shaik, A. Alamri, A.M. Aljebreen, O. Alharbi,

M.A. Almadi, F. Alhadeq, N.A. Azzam, A. Semlali, M. Alanazi, M.D. Bazzi, N. Reddy Parine, The Effect of Poly(ADP-ribose) Polymerase-1 Gene 3'Untranslated Region Polymorphism in Colorectal Cancer Risk among Saudi Cohort., Dis. Markers. 2016 (2016) 8289293. doi:10.1155/2016/8289293.

[9] H.E. Krokan, M. Bjoras, Base Excision Repair, Cold Spring Harb. Perspect. Biol. 5 (2013) a012583–a012583. doi:10.1101/cshperspect.a012583.

[10] D. Ray, D. Kidane, Gut Microbiota Imbalance and Base Excision Repair Dynamics in Colon Cancer., J. Cancer. 7 (2016) 1421–30. doi:10.7150/jca.15480.

[11] G. Antoniali, M.C. Malfatti, G. Tell, Unveiling the non-repair face of the Base Excision Repair pathway in RNA processing: A missing link between DNA repair and gene expression?, DNA Repair (Amst). 56 (2017) 65–74. doi:10.1016/j.dnarep.2017.06.008.

[12] B.D. Freudenthal, W.A. Beard, L. Perera, D.D. Shock, T. Kim, T. Schlick, S.H. Wilson, Uncovering the polymerase-induced cytotoxicity of an oxidized nucleotide, Nature. 517 (2015) 635–639. doi:10.1038/nature13886.

[13] A.M. Whitaker, T.S. Flynn, B.D. Freudenthal, Molecular snapshots of APE1 proofreading mismatches and removing DNA damage, Nat. Commun. 9 (2018) 399. doi:10.1038/s41467-017-02175-y.

[14] M.C. Malfatti, S. Balachander, G. Antoniali, K.D. Koh, C. Saint-Pierre, D. Gasparutto, H. Chon, R.J. Crouch, F. Storici, G. Tell, Abasic and oxidized ribonucleotides embedded in DNA are processed by human APE1 and not by RNase H2, Nucleic Acids Res. 45 (2017) 11193–11212. doi:10.1093/nar/gkx723.

[15] G. Tell, F. Quadrifoglio, C. Tiribelli, M.R. Kelley, The many functions of APE1/Ref-1: not only a DNA repair enzyme., Antioxid. Redox Signal. 11 (2009) 601–20. doi:10.1089/ars.2008.2194.

[16] M. Luo, J. Zhang, H. He, D. Su, Q. Chen, M.L. Gross, M.R. Kelley, M.M. Georgiadis,

Characterization of the redox activity and disulfide bond formation in apurinic/apyrimidinic endonuclease., Biochemistry. 51 (2012) 695–705. doi:10.1021/bi201034z.

[17] J. Zhang, M. Luo, D. Marasco, D. Logsdon, K.A. LaFavers, Q. Chen, A. Reed, M.R. Kelley, M.L. Gross, M.M. Georgiadis, Inhibition of apurinic/apyrimidinic endonuclease I's redox activity revisited., Biochemistry. 52 (2013) 2955–66. doi:10.1021/bi400179m.

[18] M. Luo, S. Delaplane, A. Jiang, A. Reed, Y. He, M. Fishel, R.L. Nyland, R.F. Borch, X. Qiao, M.M. Georgiadis, M.R. Kelley, M.R. Kelley, Role of the multifunctional DNA repair and redox signaling protein Ape1/Ref-1 in cancer and endothelial cells: small-molecule inhibition of the redox function of Ape1., Antioxid. Redox Signal. 10 (2008) 1853–67. doi:10.1089/ars.2008.2120.

[19] D. Su, S. Delaplane, M. Luo, D.L. Rempel, B. Vu, M.R. Kelley, M.L. Gross, M.M. Georgiadis, Interactions of apurinic/apyrimidinic endonuclease with a redox inhibitor: evidence for an alternate conformation of the enzyme., Biochemistry. 50 (2011) 82–92. doi:10.1021/bi101248s.

[20] M.M. Georgiadis, M. Luo, R.K. Gaur, S. Delaplane, X. Li, M.R. Kelley, Evolution of the redox function in mammalian apurinic/apyrimidinic endonuclease., Mutat. Res. 643 (2008) 54–63. doi:10.1016/j.mrfmmm.2008.04.008.

[21] G. Antoniali, F. Serra, L. Lirussi, M. Tanaka, C. D'Ambrosio, S. Zhang, S. Radovic, E. Dalla, Y. Ciani, A. Scaloni, M. Li, S. Piazza, G. Tell, Mammalian APE1 controls miRNA processing and its interactome is linked to cancer RNA metabolism, Nat. Commun. 8 (2017) 797. doi:10.1038/s41467-017-00842-8.

[22] M. Poletto, M.C. Malfatti, D. Dorjsuren, P.L. Scognamiglio, D. Marasco, C. Vascotto, A. Jadhav, D.J. Maloney, D.M. Wilson, A. Simeonov, G. Tell, G. Tell, Inhibitors of the apurinic/apyrimidinic endonuclease 1 (APE1)/nucleophosmin (NPM1) interaction that

display anti-tumor properties., Mol. Carcinog. 55 (2016) 688–704. doi:10.1002/mc.22313.

[23] D. Lou, L. Zhu, H. Ding, H.-Y. Dai, G.-M. Zou, Aberrant expression of redox protein Ape1 in colon cancer stem cells., Oncol. Lett. 7 (2014) 1078–1082. doi:10.3892/ol.2014.1864.

[24] T. Noike, S. Miwa, J. Soeda, A. Kobayashi, S. Miyagawa, Increased expression of thioredoxin-1, vascular endothelial growth factor, and redox factor-1 is associated with poor prognosis in patients with liver metastasis from colorectal cancer, Hum. Pathol. 39 (2008) 201–208. doi:10.1016/j.humpath.2007.04.024.

[25] E. Coskun, P. Jaruga, P.T. Reddy, M. Dizdaroglu, Extreme Expression of DNA Repair Protein Apurinic/Apyrimidinic Endonuclease 1 (APE1) in Human Breast Cancer As Measured by Liquid Chromatography and Isotope Dilution Tandem Mass Spectrometry, Biochemistry. 54 (2015) 5787–5790. doi:10.1021/acs.biochem.5b00928.

[26] V. Di Maso, M.G. Mediavilla, C. Vascotto, F. Lupo, U. Baccarani, C. Avellini, G. Tell, C. Tiribelli, L.S. Crocè, Transcriptional Up-Regulation of APE1/Ref-1 in Hepatic Tumor: Role in Hepatocytes Resistance to Oxidative Stress and Apoptosis., PLoS One. 10 (2015) e0143289. doi:10.1371/journal.pone.0143289.

[27] M.R. Kelley, L. Cheng, R. Foster, R. Tritt, J. Jiang, J. Broshears, M. Koch, Elevated and altered expression of the multifunctional DNA base excision repair and redox enzyme Ape1/ref-1 in prostate cancer., Clin. Cancer Res. 7 (2001) 824–30.

[28] Y. Jiang, S. Zhou, G.E. Sandusky, M.R. Kelley, M.L. Fishel, Reduced expression of DNA repair and redox signaling protein APE1/Ref-1 impairs human pancreatic cancer cell survival, proliferation, and cell cycle progression., Cancer Invest. 28 (2010) 885–95. doi:10.3109/07357907.2010.512816.

[29] D.H. Moore, H. Michael, R. Tritt, S.H. Parsons, M.R. Kelley, Alterations in the

expression of the DNA repair/redox enzyme APE/ref-1 in epithelial ovarian cancers., Clin. Cancer Res. 6 (2000) 602–9.

[30] D.G. Yoo, Y.J. Song, E.J. Cho, S.K. Lee, J.B. Park, J.H. Yu, S.P. Lim, J.M. Kim, B.H. Jeon, Alteration of APE1/ref-1 expression in non-small cell lung cancer: The implications of impaired extracellular superoxide dismutase and catalase antioxidant systems, Lung Cancer. 60 (2008) 277–284. doi:10.1016/j.lungcan.2007.10.015.

[31] J. Ding, M.L. Fishel, A.M. Reed, E. McAdams, M.B. Czader, A.A. Cardoso, M.R. Kelley, Ref-1/APE1 as a Transcriptional Regulator and Novel Therapeutic Target in Pediatric T-cell Leukemia, Mol. Cancer Ther. 16 (2017) 1401–1411. doi:10.1158/1535-7163.MCT-17-0099.

[32] F. Shah, D. Logsdon, R.A. Messmann, J.C. Fehrenbacher, M.L. Fishel, M.R. Kelley, Exploiting the Ref-1-APE1 node in cancer signaling and other diseases: from bench to clinic., NPJ Precis. Oncol. 1 (2017). doi:10.1038/s41698-017-0023-0.

[33] S. Zhang, L. He, N. Dai, W. Guan, J. Shan, X. Yang, Z. Zhong, Y. Qing, F. Jin, C. Chen, Y. Yang, H. Wang, L. Baugh, G. Tell, D.M. Wilson, M. Li, D. Wang, D. Wang, Serum APE1 as a predictive marker for platinum-based chemotherapy of non-small cell lung cancer patients., Oncotarget. 7 (2016) 77482–77494. doi:10.18632/oncotarget.13030.

[34] M.L. Fishel, M.R. Kelley, The DNA base excision repair protein Ape1/Ref-1 as a therapeutic and chemopreventive target, Mol. Aspects Med. 28 (2007) 375–395. doi:10.1016/j.mam.2007.04.005.

[35] G. Rai, V.N. Vyjayanti, D. Dorjsuren, A. Simeonov, A. Jadhav, D.M. Wilson, D.J. Maloney, D.J. Maloney, Synthesis, biological evaluation, and structure-activity relationships of a novel class of apurinic/apyrimidinic endonuclease 1 inhibitors., J. Med. Chem. 55 (2012) 3101–12. doi:10.1021/jm201537d.

[36] M.D. Wyatt, D.L. Pittman, Methylating Agents and DNA Repair

923 Responses: Methylated Bases and Sources of Strand Breaks, Chem. Res. Toxicol.
924 19 (2006) 1580–1594. doi:10.1021/tx060164e.
925 [37] C. Lundin, M. North, K. Erixon, K. Walters, D. Jenssen, A.S.H. Goldman, T.
926 Helleday, Methyl methanesulfonate (MMS) produces heat-labile DNA damage but
927 no detectable in vivo DNA double-strand breaks., Nucleic Acids Res. 33 (2005)
928 3799–811. doi:10.1093/nar/gki681.
929 [38] M.R. Kelley, J.H. Wikel, C. Guo, K.E. Pollok, B.J. Bailey, R. Wireman, M.L. Fishel,
930 M.R. Vasko, Identification and Characterization of New Chemical Entities Targeting
931 Apurinic/Apyrimidinic Endonuclease 1 for the Prevention of Chemotherapy-Induced
932 Peripheral Neuropathy., J. Pharmacol. Exp. Ther. 359 (2016) 300–309.
933 doi:10.1124/jpet.116.235283.
934 [39] M.L. Fishel, Y. Jiang, N. V. Rajeshkumar, G. Scandura, A.L. Sinn, Y. He, C. Shen,
935 D.R. Jones, K.E. Pollok, M. Ivan, A. Maitra, M.R. Kelley, Impact of APE1/Ref-1
936 Redox Inhibition on Pancreatic Tumor Growth, Mol. Cancer Ther. 10 (2011) 1698–
937 1708. doi:10.1158/1535-7163.MCT-11-0107.
938 [40] A.A. Cardoso, Y. Jiang, M. Luo, A.M. Reed, S. Shahda, Y. He, A. Maitra, M.R.
939 Kelley, M.L. Fishel, APE1/Ref-1 regulates STAT3 transcriptional activity and
940 APE1/Ref-1-STAT3 dual-targeting effectively inhibits pancreatic cancer cell survival.,
941 PLoS One. 7 (2012) e47462. doi:10.1371/journal.pone.0047462.
942 [41] S.S. Laev, N.F. Salakhutdinov, O.I. Lavrik, Inhibitors of nuclease and redox activity
943 of apurinic/apyrimidinic endonuclease 1/redox effector factor 1 (APE1/Ref-1).,
944 Bioorg. Med. Chem. 25 (2017) 2531–2544. doi:10.1016/j.bmc.2017.01.028.
945 [42] M.R.K. afi Shahda, Nehal J. Lakhani, Bert O'Neil, Drew W. Rasco, Jun Wan, Amber
946 L Mosley, Hao Liu, A phase I study of the APE1 protein inhibitor APX3330 in
947 patients with advanced solid tumors. | 2019 ASCO Annual Meeting Abstracts,
948 (2019). http://abstracts.asco.org/239/AbstView_239_257841.html (accessed May 30,

2019).

[43] R.A.M. incy Chu, Amanda K. L. Anderson, Mark Andrew Landers, Yipeng Wang, Mark R. Kelley, CTC enumeration and characterization as a pharmacodynamic marker in the phase I clinical study of APX3330, an APE1/Ref-1 inhibitor, in patients with advanced solid tumors. | 2019 ASCO Annual Meeting Abstracts, (2019). http://abstracts.asco.org/239/AbstView_239_257889.html (accessed May 30, 2019).

[44] W. Zhao, D. Li, Z. Liu, X. Zheng, J. Wang, E. Wang, Spiclomazine induces apoptosis associated with the suppression of cell viability, migration and invasion in pancreatic carcinoma cells., PLoS One. 8 (2013) e66362. doi:10.1371/journal.pone.0066362.

[45] A. Cristobal, H.W.P. van den Toorn, M. van de Wetering, H. Clevers, A.J.R. Heck, S. Mohammed, Personalized Proteome Profiles of Healthy and Tumor Human Colon Organoids Reveal Both Individual Diversity and Basic Features of Colorectal Cancer., Cell Rep. 18 (2017) 263–274. doi:10.1016/j.celrep.2016.12.016.

[46] Y. Ohta, T. Sato, Intestinal tumor in a dish., Front. Med. 1 (2014) 14. doi:10.3389/fmed.2014.00014.

[47] E.R. Kastenhuber, S.W. Lowe, Putting p53 in Context., Cell. 170 (2017) 1062–1078. doi:10.1016/j.cell.2017.08.028.

[48] X.-L. Li, J. Zhou, Z.-R. Chen, W.-J. Chng, P53 mutations in colorectal cancer - molecular pathogenesis and pharmacological reactivation., World J. Gastroenterol. 21 (2015) 84–93. doi:10.3748/wjg.v21.i1.84.

[49] B. Iacopetta, A. Russo, V. Bazan, G. Dardanoni, N. Gebbia, T. Soussi, D. Kerr, H. Elsaleh, R. Soong, D. Kandioler, E. Janschek, S. Kappel, M. Lung, C.-S.S. Leung, J.M. Ko, S. Yuen, J. Ho, S.Y. Leung, E. Crapez, J. Duffour, M. Ychou, D.T. Leahy, D.P. O'Donoghue, V. Agnese, S. Cascio, G. Di Fede, L. Chieco-Bianchi, R. Bertorelle, C. Belluco, W. Giaretti, P. Castagnola, E. Ricevuto, C. Ficorella, S. Bosari, C.D. Arizzi, M. Miyaki, M. Onda, E. Kampman, B. Diergaarde, J. Royds, R.A.

975 Lothe, C.B. Diep, G.I. Meling, J. Ostrowski, L. Trzeciak, K. Guzińska-Ustymowicz, B.
976 Zalewski, G.M. Capellá, V. Moreno, M.A. Peinado, C. Lönnroth, K. Lundholm, X.F.
977 Sun, A. Jansson, H. Bouzourene, L.-L. Hsieh, R. Tang, D.R. Smith, T.G. Allen-
978 Mersh, Z.A.J. Khan, A.J. Shorthouse, M.L. Silverman, S. Kato, C. Ishioka, TP53-
979 CRC Collaborative Group, Functional categories of TP53 mutation in colorectal
980 cancer: results of an International Collaborative Study, Ann. Oncol. 17 (2006) 842–
981 847. doi:10.1093/annonc/mdl035.
982 [50] S.L. Harris, A.J. Levine, The p53 pathway: positive and negative feedback loops,
983 Oncogene. 24 (2005) 2899–2908. doi:10.1038/sj.onc.1208615.
984 [51] A.B. Williams, B. Schumacher, p53 in the DNA-Damage-Repair Process., Cold
985 Spring Harb. Perspect. Med. 6 (2016). doi:10.1101/cshperspect.a026070.
986 [52] A. Chatterjee, E. Mambo, M. Osada, S. Upadhyay, D. Sidransky, The effect of *p53* -
987 RNAi and *p53* knockout on human 8-oxoguanine DNA glycosylase (hOgg1) activity,
988 FASEB J. 20 (2006) 112–114. doi:10.1096/fj.04-3423fje.
989 [53] S. Oka, J. Leon, D. Tsuchimoto, K. Sakumi, Y. Nakabeppu, MUTYH, an adenine
990 DNA glycosylase, mediates p53 tumor suppression via PARP-dependent cell death,
991 Oncogenesis. 3 (2014) e121–e121. doi:10.1038/oncsis.2014.35.
992 [54] Y. Cun, N. DAI, M. LI, C. XIONG, Q. ZHANG, J. SUI, C. QIAN, D. WANG,
993 APE1/Ref-1 enhances DNA binding activity of mutant p53 in a redox-dependent
994 manner, Oncol. Rep. 31 (2014) 901–909. doi:10.3892/or.2013.2892.
995 [55] A. Zaky, C. Busso, T. Izumi, R. Chattopadhyay, A. Bassiouny, S. Mitra, K.K. Bhakat,
996 Regulation of the human AP-endonuclease (APE1/Ref-1) expression by the tumor
997 suppressor p53 in response to DNA damage, Nucleic Acids Res. 36 (2008) 1555–
998 1566. doi:10.1093/nar/gkm1173.
999 [56] J. Zhou, J. Ahn, S.H. Wilson, C. Prives, A role for p53 in base excision repair, EMBO
1000 J. 20 (2001) 914–923. doi:10.1093/emboj/20.4.914.

[57] G. Antoniali, F. Marcuzzi, E. Casarano, G. Tell, Cadmium treatment suppresses DNA polymerase δ catalytic subunit gene expression by acting on the p53 and Sp1 regulatory axis, DNA Repair (Amst). 35 (2015) 90–105. doi:10.1016/j.dnarep.2015.08.007.

[58] M. Fujii, M. Shimokawa, S. Date, A. Takano, M. Matano, K. Nanki, Y. Ohta, K. Toshimitsu, Y. Nakazato, K. Kawasaki, T. Uraoka, T. Watanabe, T. Kanai, T. Sato, A Colorectal Tumor Organoid Library Demonstrates Progressive Loss of Niche Factor Requirements during Tumorigenesis., Cell Stem Cell. 18 (2016) 827–38. doi:10.1016/j.stem.2016.04.003.

[59] Q. Meng, S. Shi, C. Liang, D. Liang, W. Xu, S. Ji, B. Zhang, Q. Ni, J. Xu, X. Yu, Diagnostic and prognostic value of carcinoembryonic antigen in pancreatic cancer: a systematic review and meta-analysis., Onco. Targets. Ther. 10 (2017) 4591–4598. doi:10.2147/OTT.S145708.

[60] M. Comelli, I. Pretis, A. Buso, I. Mavelli, Mitochondrial energy metabolism and signalling in human glioblastoma cell lines with different PTEN gene status, J. Bioenerg. Biomembr. 50 (2018) 33–52. doi:10.1007/s10863-017-9737-5.

[61] D. Risso, J. Ngai, T.P. Speed, S. Dudoit, Normalization of RNA-seq data using factor analysis of control genes or samples, Nat. Biotechnol. 32 (2014) 896–902. doi:10.1038/nbt.2931.

[62] D.W. Huang, B.T. Sherman, R.A. Lempicki, Systematic and integrative analysis of large gene lists using DAVID bioinformatics resources, Nat. Protoc. 4 (2009) 44–57. doi:10.1038/nprot.2008.211.

[63] P.B. Marcin Kosinski, Bioconductor - RTCGA, (n.d.). doi:10.18129/B9.bioc.RTCGA.

[64] S. Kakolyris, L. Kaklamanis, K. Engels, H. Turley, I.D. Hickson, K.C. Gatter, A.L. Harris, Human apurinic endonuclease 1 expression in a colorectal adenoma-carcinoma sequence., Cancer Res. 57 (1997) 1794–7.

[65] F. Bunz, A. Dutriaux, C. Lengauer, T. Waldman, S. Zhou, J.P. Brown, J.M. Sedivy, K.W. Kinzler, B. Vogelstein, Requirement for p53 and p21 to sustain G2 arrest after DNA damage., Science. 282 (1998) 1497–501. doi:10.1126/science.282.5393.1497.

[66] S. Masani, L. Han, K. Yu, Apurinic/apyrimidinic endonuclease 1 is the essential nuclease during immunoglobulin class switch recombination., Mol. Cell. Biol. 33 (2013) 1468–73. doi:10.1128/MCB.00026-13.

[67] M. Poletto, A.J. Legrand, S.C. Fletcher, G.L. Dianov, p53 coordinates base excision repair to prevent genomic instability, Nucleic Acids Res. 44 (2016) 3165–3175. doi:10.1093/nar/gkw015.

[68] M. Christmann, B. Kaina, Transcriptional regulation of human DNA repair genes following genotoxic stress: trigger mechanisms, inducible responses and genotoxic adaptation, Nucleic Acids Res. 41 (2013) 8403–8420. doi:10.1093/nar/gkt635.

[69] B. Li, M.Y. Lee, Transcriptional regulation of the human DNA polymerase delta catalytic subunit gene POLD1 by p53 tumor suppressor and Sp1., J. Biol. Chem. 276 (2001) 29729–39. doi:10.1074/jbc.M101167200.

[70] T. Sutcliffe, L. Fu, J. Abraham, H. Vaziri, S. Benchimol, A functional wild-type p53 gene is expressed in human acute myeloid leukemia cell lines., Blood. 92 (1998) 2977–9.

[71] N. Shtraizent, H. Matsui, A. Polotskaia, J. Bargonetti, Hot Spot Mutation in TP53 (R248Q) Causes Oncogenic Gain-of-Function Phenotypes in a Breast Cancer Cell Line Derived from an African American patient., Int. J. Environ. Res. Public Health. 13 (2015) ijerph13010022. doi:10.3390/ijerph13010022.

[72] B. Plitzko, S. Loesgen, Measurement of Oxygen Consumption Rate (OCR) and Extracellular Acidification Rate (ECAR) in Culture Cells for Assessment of the Energy Metabolism, BIO-PROTOCOL. 8 (2018). doi:10.21769/BioProtoc.2850.

[73] T. Yamamori, J. DeRicco, A. Naqvi, T.A. Hoffman, I. Mattagajasingh, K. Kasuno, S.-

B. Jung, C.-S. Kim, K. Irani, SIRT1 deacetylates APE1 and regulates cellular base excision repair, Nucleic Acids Res. 38 (2010) 832–845. doi:10.1093/nar/gkp1039.

[74] T. Lindahl, D.E.E. Barnes, Repair of endogenous DNA damage., Cold Spring Harb. Symp. Quant. Biol. 65 (2000) 127–33. doi:10.1101/sqb.2000.65.127.

[75] M.-O. Turgeon, N.J.S. Perry, G. Poulogiannis, DNA Damage, Repair, and Cancer Metabolism., Front. Oncol. 8 (2018) 15. doi:10.3389/fonc.2018.00015.

[76] D.W. Meek, Tumour suppression by p53: a role for the DNA damage response?, Nat. Rev. Cancer. 9 (2009) 714–723. doi:10.1038/nrc2716.

[77] R. Ali, E.A. Rakha, S. Madhusudan, H.E. Bryant, DNA damage repair in breast cancer and its therapeutic implications, Pathology. 49 (2017) 156–165. doi:10.1016/j.pathol.2016.11.002.

[78] M.-A.M. Mattar, A.-R.N. Zekri, N. Hussein, H. Morsy, G. Esmat, M.A. Amin, Polymorphisms of base-excision repair genes and the hepatocarcinogenesis, Gene. 675 (2018) 62–68. doi:10.1016/j.gene.2018.06.056.

[79] R. Abbotts, R. Jewell, J. Nsengimana, D.J. Maloney, A. Simeonov, C. Seedhouse, F. Elliott, J. Laye, C. Walker, A. Jadhav, A. Grabowska, G. Ball, P.M. Patel, J. Newton-Bishop, D.M. Wilson, S. Madhusudan, Targeting human apurinic/apyrimidinic endonuclease 1 (APE1) in phosphatase and tensin homolog (PTEN) deficient melanoma cells for personalized therapy., Oncotarget. 5 (2014) 3273–86. doi:10.18632/oncotarget.1926.

[80] M. Kumar, V.K. Shukla, P.K. Misra, M.J. Raman, Dysregulated Expression and Subcellular Localization of Base Excision Repair (BER) Pathway Enzymes in Gallbladder Cancer., Int. J. Mol. Cell. Med. 7 (2018) 119–132. doi:10.22088/IJMCM.BUMS.7.2.119.

[81] D.B. Azambuja, N.M. Leguisamo, H.C. Gloria, A.N. Kalil, E. Rhoden, J. Saffi, Prognostic impact of changes in base excision repair machinery in sporadic

colorectal cancer, Pathol. - Res. Pract. 214 (2018) 64–71. doi:10.1016/j.prp.2017.11.012.

[82] S. Vodenkova, K. Jiraskova, M. Urbanova, M. Kroupa, J. Slyskova, M. Schneiderova, M. Levy, T. Buchler, V. Liska, L. Vodickova, V. Vymetalkova, A. Collins, A. Opattova, P. Vodicka, Base excision repair capacity as a determinant of prognosis and therapy response in colon cancer patients, DNA Repair (Amst). 72 (2018) 77–85. doi:10.1016/j.dnarep.2018.09.006.

[83] G.-M. Zou, C. Karikari, Y. Kabe, H. Handa, R.A. Anders, A. Maitra, The Ape-1/Ref-1 redox antagonist E3330 inhibits the growth of tumor endothelium and endothelial progenitor cells: Therapeutic implications in tumor angiogenesis, J. Cell. Physiol. 219 (2009) 209–218. doi:10.1002/jcp.21666.

[84] G.-M. Zou, A. Maitra, Small-molecule inhibitor of the AP endonuclease 1/REF-1 E3330 inhibits pancreatic cancer cell growth and migration, Mol. Cancer Ther. 7 (2008) 2012–2021. doi:10.1158/1535-7163.MCT-08-0113.

[85] D.P. Logsdon, F. Shah, F. Carta, C.T. Supuran, M. Kamocka, M.H. Jacobsen, G.E. Sandusky, M.R. Kelley, M.L. Fishel, Blocking HIF signaling via novel inhibitors of CA9 and APE1/Ref-1 dramatically affects pancreatic cancer cell survival, Sci. Rep. 8 (2018) 13759. doi:10.1038/s41598-018-32034-9.

[86] P.S. Guerreiro, E. Corvacho, J.G. Costa, N. Saraiva, A.S. Fernandes, M. Castro, J.P. Miranda, N.G. Oliveira, The APE1 redox inhibitor E3330 reduces collective cell migration of human breast cancer cells and decreases chemoinvasion and colony formation when combined with docetaxel, Chem. Biol. Drug Des. 90 (2017) 561–571. doi:10.1111/cbdd.12979.

[87] Y. Saitou, K. Shiraki, T. Yamanaka, K. Miyashita, T. Inoue, Y. Yamanaka, Y. Yamaguchi, N. Enokimura, N. Yamamoto, K. Itou, K. Sugimoto, T. Nakano, Augmentation of tumor necrosis factor family-induced apoptosis by E3330 in human

hepatocellular carcinoma cell lines via inhibition of NF kappa B., World J. Gastroenterol. 11 (2005) 6258–61. doi:10.3748/wjg.v11.i40.6258.

[88] D.W. McIlwain, M.L. Fishel, A. Boos, M.R. Kelley, T.J. Jerde, APE1/Ref-1 redox-specific inhibition decreases survivin protein levels and induces cell cycle arrest in prostate cancer cells, Oncotarget. 9 (2018) 10962–10977. doi:10.18632/oncotarget.23493.

[89] J. Fields, J.J. Hanisch, J.W. Choi, P.M. Hwang, Is There an Answer? How Does p53 Regulate Mitochondrial Respiration?, (n.d.). doi:10.1080/15216540601185021.

[90] N. Hashimoto, H. Nagano, T. Tanaka, The role of tumor suppressor p53 in metabolism and energy regulation, and its implication in cancer and lifestyle-related diseases, Endocr. J. 66 (2019) 485–496. doi:10.1507/endocrj.EJ18-0565.

[91] J.-H. Park, J. Zhuang, J. Li, P.M. Hwang, p53 as guardian of the mitochondrial genome, FEBS Lett. 590 (2016) 924. doi:10.1002/1873-3468.12061.

[92] G. Tell, E. Crivellato, A. Pines, I. Paron, C. Pucillo, G. Manzini, A. Bandiera, M.R. Kelley, C. Di Loreto, G. Damante, Mitochondrial localization of APE/Ref-1 in thyroid cells., Mutat. Res. 485 (2001) 143–52. doi:10.1016/s0921-8777(00)00068-9.

[93] R. Chattopadhyay, L. Wiederhold, B. Szczesny, I. Boldogh, T.K. Hazra, T. Izumi, S. Mitra, Identification and characterization of mitochondrial abasic (AP)-endonuclease in mammalian cells, Nucleic Acids Res. 34 (2006) 2067. doi:10.1093/NAR/GKL177.

[94] H.K. Joo, Y.R. Lee, M.S. Park, S. Choi, K. Park, S.K. Lee, C.-S. Kim, J.B. Park, B.H. Jeon, Mitochondrial APE1/Ref-1 suppressed protein kinase C-induced mitochondrial dysfunction in mouse endothelial cells, Mitochondrion. 17 (2014) 42–49. doi:10.1016/J.MITO.2014.05.006.

[95] D.C. Wallace, Mitochondria and cancer, Nat. Rev. Cancer. 12 (2012) 685–698. doi:10.1038/nrc3365.

[96] A. Carracedo, L.C. Cantley, P.P. Pandolfi, Cancer metabolism: fatty acid oxidation in

1131 the limelight, Nat. Rev. Cancer. 13 (2013) 227–232. doi:10.1038/nrc3483.
1132 [97] H.-C. Kim, J. Chang, H.S. Lee, H.J. Kwon, Mitochondrial UQCRB as a new
1133 molecular prognostic biomarker of human colorectal cancer, Exp. Mol. Med. 49
1134 (2017) e391–e391. doi:10.1038/emm.2017.152.
1135 [98] C. Vascotto, L. Cesaratto, L.A.H. Zeef, M. Deganuto, C. D'Ambrosio, A. Scaloni, M.
1136 Romanello, G. Damante, G. Taglialatela, D. Delneri, M.R. Kelley, S. Mitra, F.
1137 Quadrifoglio, G. Tell, Genome-wide analysis and proteomic studies reveal
1138 APE1/Ref-1 multifunctional role in mammalian cells., Proteomics. 9 (2009) 1058–74.
1139 doi:10.1002/pmic.200800638.
1140 [99] W. Stünkel, B.K. Peh, Y.C. Tan, V.M. Nayagam, X. Wang, M. Salto-Tellez, B. Ni, M.
1141 Entzeroth, J. Wood, Function of the SIRT1 protein deacetylase in cancer,
1142 Biotechnol. J. 2 (2007) 1360–1368. doi:10.1002/biot.200700087.
1143 [100] R. Bayat Mokhtari, T.S. Homayouni, N. Baluch, E. Morgatskaya, S. Kumar, B. Das,
1144 H. Yeger, Combination therapy in combating cancer., Oncotarget. 8 (2017) 38022–
1145 38043. doi:10.18632/oncotarget.16723.
1146

Table

Model used	Drug	Time (hours)	IC_{50} (∝M)	Assay
$CH12F3^{+/+/\Delta}$	Compound #3	48	1.44	CellTiter
$^{\Delta/\Delta/\Delta}CH12F3$			1.9	
HCT-116 $p53^{+/+}$			0.58	MTS
HCT-116 $p53^{-/-}$			0.69	
HCT-116 $p53^{+/+}$			1.04	RealTime-Glo
HCT-116 $p53^{-/-}$			1.50	
$CH12F3^{+/+/\Delta}$	APX2009		6.61	CellTiter
$^{\Delta/\Delta/\Delta}CH12F3$			9.64	
HCT-116 $p53^{+/+}$			11.7	MTS
HCT-116 $p53^{-/-}$			11.6	
HCT-116 $p53^{+/+}$			10.0	RealTime-Glo
HCT-116 $p53^{-/-}$			6.39	
HCT-116 $p53^{+/+}$	Fiduxosin		16.1	MTS
HCT-116 $p53^{-/-}$			15.6	
HCT-116 $p53^{+/+}$	SB206553		n.d. (>100)	
HCT-116 $p53^{-/-}$			n.d. (>100)	
HCT-116 $p53^{+/+}$	Spiclomazine		30.4	
HCT-116 $p53^{-/-}$			31.2	
HCT-116 $p53^{+/+}$	MMS	8	721	
HCT-116 $p53^{-/-}$			938	
HCT-116 $p53^{+/+}$	Compound #3	40 + 8	0.373	
HCT-116 $p53^{-/-}$			0.58	
tumor organoid P12	Compound #3	48	1.36	RealTime-Glo
tumor organoid P14			2.8	
tumor organoid P16			0.71	

Table 1: List of IC_{50} values obtained from each model used. The analysis was carried out using the Combenefit 2.021 software allowing to calculate the IC_{50} values for each drug tested on the models analyzed. Cell models (cell lines and patient-derived 3D tumor organoids), types of assays, drugs and time points are reported. n.d. indicates that the goodness of fit value is too low or a standard Hill equation does not correctly account for the specific agent used. In some cases, the expected interpolated IC_{50} value has been reported.

Figure legends

Fig. 1. APE1 is overexpressed in colorectal cancer and the inhibition of its endonuclease activity triggers p53-mediated effects on cell metabolism.

(**A**) Gene expression level of *APEX1* in the CRC samples of the four CMS classes and normal controls (CMS1 MSI Immune n=71; CMS2 Canonical n=130; CMS3 Metabolic n=58; CMS4 Mesenchymal n=98; control n=42). For left to right, the violin plots illustrate the log(FPKM+1) normalized gene expression level in the CMS 1-4 class CRC and normal control samples, respectively. (**B**) Schematic representation of different functions of APE1. The specific inhibitors of the different functions of APE1 are also indicated. (**C**) Western blot analysis of p53 and APE1 protein levels in HCT116 $p53^{+/+}$ and $p53^{-/-}$ cell lines. Actin was used as a loading control. MTS assay on HCT-116 $p53^{+/+}$ and $p53^{-/-}$ cell lines. Cells were treated with increasing amounts of APE1 inhibitors (Compound #3, APX2009, Fiduxosin, SB206553 and Spiclomazine) at the indicated concentrations for 48 h. Untreated cells were treated with DMSO. In graph, the percentage of metabolic activity relative to untreated cells, arbitrary set to 100%, is represented. Values are mean±SD ($n \geq 3$). (**D**) RealTime Glo assay on HCT-116 $p53^{+/+}$ and $p53^{-/-}$ cell lines. Cells were treated with increasing amounts of Compound #3 or APX2009 for 48 h. Untreated cells were treated with DMSO. In graph, the percentage of metabolic activity relative to untreated cells, arbitrary set to 100%, is represented. Values are mean±SD (n=3). (**E**) Western blot analysis of APE1 in $CH12F3^{+/+/\Delta}$ and $CH12F3^{\Delta/\Delta/\Delta}$ cell lines. Actin was used as a loading control. CellTiter assay on $CH12F3^{+/+/\Delta}$ and $CH12F3^{\Delta/\Delta/\Delta}$ cell lines. Cells were treated with increasing amounts of Compound #3 or APX2009 at the indicated concentrations for 48 h. The percentages of viable cells relative to untreated cells, arbitrary set to 100%, are represented in graph. Values are mean±SD (n=3). Data were evaluated statistically by two-tails Student t-test. Resulting p-value is indicated (* $p<0.05$, ** $p<0.01$, *** $p<0.005$).

Fig. 2. Inhibition of APE1-endonuclease activity promotes p53 activation.

HCT-116 $p53^{+/+}$ and $p53^{-/-}$ cell lines were treated with Compound #3 (#3) at the indicated concentrations for 48h. Untreated cells were treated with DMSO (**A**-**F, L**). (**A**) The amount of abasic (AP) sites was measurement. Values are mean±SD (n=3). (**B**) Representative fluorescence confocal microscope images of *in vitro* comet assay. Scale bars,25 μm. (**C**) Tail moment was analysed for 100 cells at random by OpenComet software. Untreated cells was used as reference and set to 1. Values are mean±SD. (**D**) Western blot analysis of p53, p21, APE1 and Nucleophosmin (NPM1) protein levels. Actin was used as a loading control (n=3). (**E**) Densitometric analysis of p53, p21, APE1 and NPM1 protein expression. Levels were normalized to actin. Fold change values relative to untreated control cells, arbitrary set to 100%, are shown. Values are mean±SD (n=3). (**F**) Expression level of DNA Polimerase δ (DNA Pol δ) was determined by qRT-PCR analysis. DNA Pol δ levels were normalized to β-actin. Fold change values relative to untreated control cells, arbitrary set to 1, are shown. Values are mean±SD (n=3). (**G**) HCT116 $p53^{+/+}$ cell lines silenced for APE1 expression. Western blot analysis of p53 and APE1 protein levels. Actin was used as a loading control. Fold change values relative to untreated control cells, arbitrary set to 1, are shown. (**H** and **I**) Western blot analysis of p53 protein levels upon Compound #3 (#3) at the indicated concentrations of AML2 cell lines treated with for 48 h (**H**) and HCC70 cell lines treated for 24 h (**I**). Actin was used as a loading control. Fold change values relative to untreated control cells, arbitrary set to 1, are shown (n=3). (**L**) Apo-ONE assay was used to quantify relative levels of apoptosis. The activities of caspases 3/7 were examined using a fluorescence-based assay. Untreated control cells were used as reference and set to 100%. Values are mean±SD (n=2). Data were evaluated statistically by two-tails Student t-test. Resulting p-value is indicated (* $p<0.05$, ** $p<0.01$).

Fig. 3. Inhibition of APE1-redox activity does not affect p53 expression.

HCT-116 $p53^{+/+}$ and HCT-116 $p53^{-/-}$ cells were treated with APX2009 (APX) at the indicated concentrations for 48h. Untreated cells were treated with DMSO. (**A**) Expression level of BIRC5 was determined by qRT-PCR analysis. BIRC5 levels were normalized to β-actin. Fold change expression values relative to untreated cells, arbitrary set to 1, are shown. Values are mean±SD (n=3). (**B**) Western blot analysis of p53, p21, APE1 and Nucleophosmin (NPM1) protein levels. Actin was used as a loading control (n=3). (**C**) Densitometric analysis of p53, p21, APE1 and NPM1 protein expression. Levels were normalized to actin. Fold change values relative to untreated control cells, arbitrary set to 100%, are shown. Values are mean±SD (n=3). (**D**) Expression level of DNA Polimerase δ (DNA Pol δ) was determined by qRT-PCR analysis. DNA Pol δ levels were normalized to β-actin. Fold change expression values relative to untreated control cells, arbitrary set to 1, are shown. Values are mean±SD (n=3). (**E**) Apo-ONE assay was used to quantify relative levels of apoptosis. The activities of caspases 3/7 were examined using a fluorescence-based assay. Untreated control cells were used as reference and set to 100%. Values are mean±SD (n=3). Data were evaluated statistically by two-tails Student t-test. Resulting p-value is indicated (* $p<0.05$, ** $p<0.01$).

Fig. 4. Inhibition of APE1-endonuclease activity impairs mitochondrial activity in a p53-dependent manner.

(**A** and **B**) HCT-116 $p53^{+/+}$ and $p53^{-/-}$ cells were seeded in a Seahorse XF-24 analyzer and treated with 0.5 μM of Compund#3 for 48 h. Untreated cells were treated with DMSO. (**A**) Real-time oxygen consumption rate (OCR) was determined during sequential treatments with oligomycin (ATP-synthase inhibitor), FCCP (uncoupler of oxidative phosphorylation),

rotenone (complex I inhibitor) and antimycin-A (complex III inhibitor). (**B**) The rates of basal respiration, ATP-coupled respiration, spare respiratory capacity and maximal respiration were quantified by normalization of OCR level to total protein content. Data represent means±SEM (n=3). Data were evaluated statistically by two-tails Student t-test. Resulting p-value is indicated (* $p<0.05$, *** $p<0.005$).

Fig. 5. Inhibition of APE1-endonuclease activity sensitises p53 expressing cell lines to MMS treatment.

MTS assay on HCT-116 $p53^{+/+}$ and HCT-116 $p53^{-/-}$ cells. Cells were treated with Compound #3 (#3) at the indicated concentrations for 40 h and in combination with 200 μM (**A**), 400 μM (**B**) or 600 μM (**C**) methyl methanesulfonate (MMS) for additional 8 h. Untreated cells were treated with DMSO. In graph, the percentage of metabolic activity relative to untreated cells, arbitrary set to 100%, is represented. Values are mean±SD (n=3). Data were evaluated statistically by two-tails Student t-test. Resulting p-value is indicated (* $p<0.05$, ** $p<0.01$).

Fig. 6. Inhibition of APE1-endonuclease activity exerts toxic effects on patient-derived tumor organoids metabolism and is associated with the p53 mutational status.

(**A**) Fluorescence confocal microscope imaging of patient-derived organoids. Patient-derived organoids were stained with Ki67 (proliferating cells), OLFM4 (intestinal stem cell), E-Cadherin (intestinal epithelial cells) or Lysozyme (Paneth cells). F-actin was stained with Phalloidin. Nuclei were visualized with DAPI. Scale bars, 50 μm (Ki67 and Lysozyme) and 25 μm (OLFM4 and E-Cadherin). (**B**) Brightfield representative images of colorectal cancer organoids derived from different patients (P12, P14 and P16). Scale bars, 200 μm. (**C**) *TP53* mutational status in colorectal cancer organoids was assessed by NGS. Patient P12, represented by the green box, harboured a wild-type p53, patient P14, represented by the

blue box, beared a stop-gain mutation while patient P16, represented by the orange box, harboured a missense one. (**D**) Western blot analysis of p53 protein level in CRC patient-derived organoids. The graph shows the densitometric analysis of p53 protein expression in patient-derived organoids. Fold change values relative to P12, arbitrary set to 1, are shown. Values are mean of 3 measurements±SD. (**E**) Western blot analysis of APE1 protein level in CRC patient-derived organoids. The graph shows the densitometric analysis of APE1 protein expression in patient-derived organoids. Fold change values relative to P12, arbitrary set to 1, are shown. Values are mean of 3 measurements±SD. (**F**) RealTime-Glo assay on patient-derived tumor organoids. Patient-derived tumor organoids were treated with increasing amounts of Compound #3 (range from 0.5 μM to 5 μM) for 48 h. In graph, the percentage of metabolic activity relative to untreated organoids, arbitrary set to 100%, is represented (n=1). Values are mean of 5 measurements±SD.

Fig. 7. Differentially expressed interactors of APE1 in colorectal cancer.

(**A**) Differentially expressed genes (DEGs) coding APE1 interactors in colon cancer (COAD) are in the middle. Cellular locations of upregulated interactors in upper panel and downregulated interactors in lower panel. The colour codes are as follows: green colour for up-regulation, orange colour for down-regulation, blue colour for mitochondrial location and grey colour for other cellular locations. (**B**) Representation of DEGs on mitochondrial scheme. Grey shaded boxes indicate mitochondrial locations while boxes without any shade indicate enriched pathways. Green upside arrows indicate up-regulation while red downside arrows indicate down-regulation. Genes that were also regulated in previously published microarray data were shown in red circles. Poor prognostic interactors were marked with circled skull symbol.

Fig. S1. APE1 mRNA and protein levels remain stable in basal condition and upon APE1 endonuclease inhibition in colon cancer cell lines.

(**A**) Expression level of APE1 were determined by qRT-PCR analysis. APE1 levels were normalized to β-actin. Fold change expression values relative to HCT-116 $p53^{+/+}$ cells, arbitrary set to 1, are shown. Values are mean±SD (n=3). (**B**) Densitometric analysis of basal APE1 expression. Levels were normalized to actin. HCT-116 $p53^{+/+}$ cells were used as reference and set to 100%. Values are mean±SD (n=6). (**C**) HCT116 $p53^{+/+}$ and HCT116 $p53^{-/-}$ cells were treated with Compound #3 (#3) at the indicated concentration for 48 h. Expression level of APE1 were determined by qRT-PCR analysis. APE1 levels were normalized to β-actin. Fold change expression values relative to untreated control cells, arbitrary set to 1, are shown. Values are mean±SD (n=3).The p-value was calculated using Student's two-tailed t-test. Resulting p-value is indicated (NS, not significant).

Fig. S2. Inhibition of APE1-endonuclease activity impairs mitochondrial activity in a p53-dependent manner.

HCT-116 $p53^{+/+}$ and HCT-116 $p53^{-/-}$ cells were seeded in a Seahorse XF-24 analyzer and treated with 0.25 μM (**A**) and 1 μM (**B**) of Compound #3 at the indicated concentrations for 48 h. Untreated cells were treated with DMSO. Real-time oxygen consumption rate (OCR) was determined during sequential treatments with oligomycin (ATP-synthase inhibitor), FCCP (uncoupler of oxidative phosphorylation), rotenone (complex I inhibitor) and antimycin-A (complex III inhibitor). Values are mean of 5 measurements±SD.

Figure 1

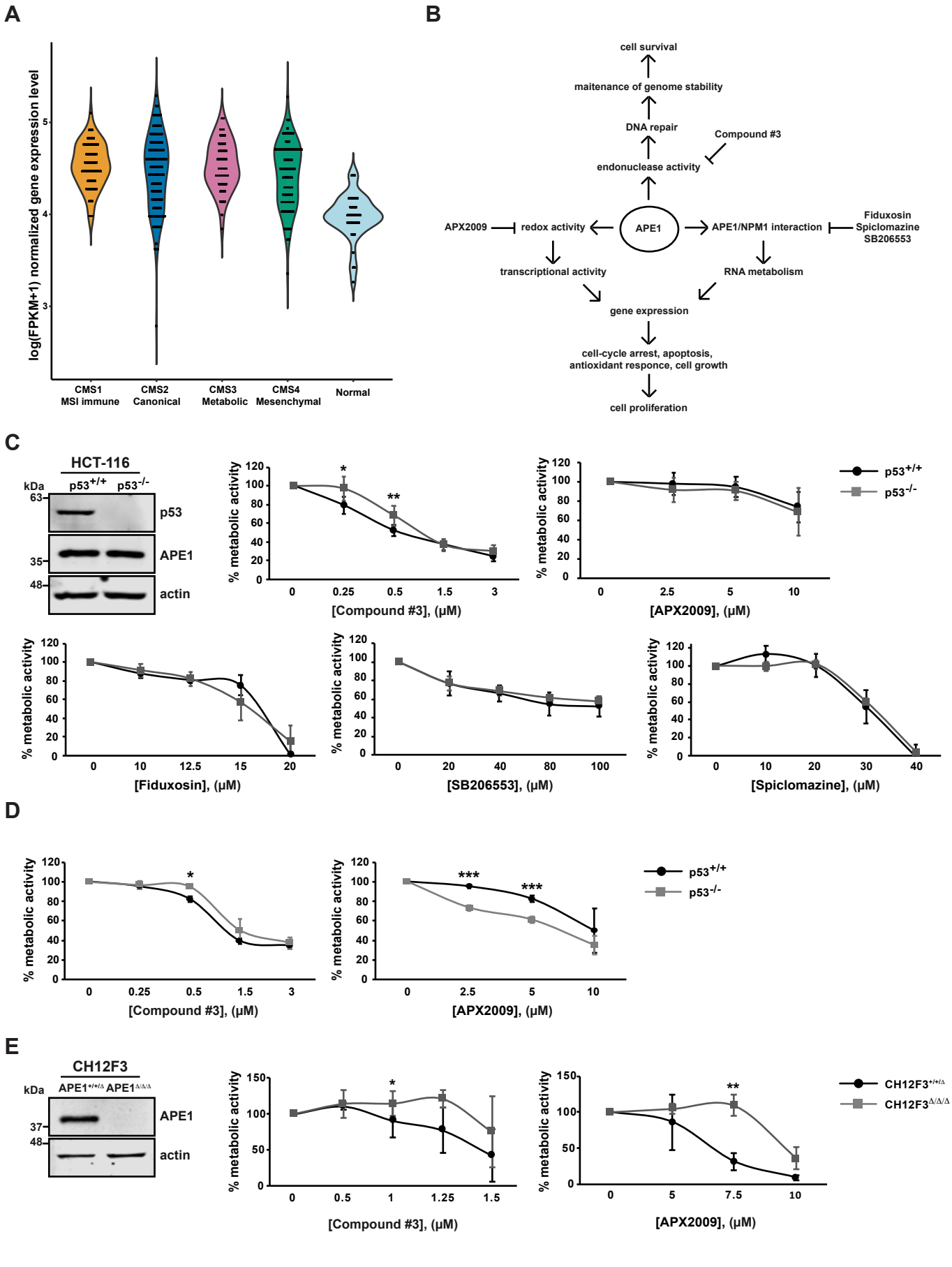
A
log(FPKM+1) normalized gene expression level
CMS1 MSI immune
CMS2 Canonical
CMS3 Metabolic
CMS4 Mesenchymal
Normal
B
cell survival
maitenance of genome stability
DNA repair
Compound #3
endonuclease activity
APX2009
redox activity
APE1
APE1/NPM1 interaction
Fiduxosin
Spiclomazine
SB206553
transcriptional activity
RNA metabolism
gene expression
cell-cycle arrest, apoptosis, antioxidant responce, cell growth
cell proliferation
C
HCT-116
kDa
p53+/+
p53-/-
63
35
48
p53
APE1
actin
% metabolic activity
[Compound #3], (μM)
[APX2009], (μM)
[Fiduxosin], (μM)
[SB206553], (μM)
[Spiclomazine], (μM)
D
E
CH12F3
APE1+/+Δ
APE1Δ/Δ/Δ
37
CH12F3+/+Δ
CH12F3Δ/Δ/Δ

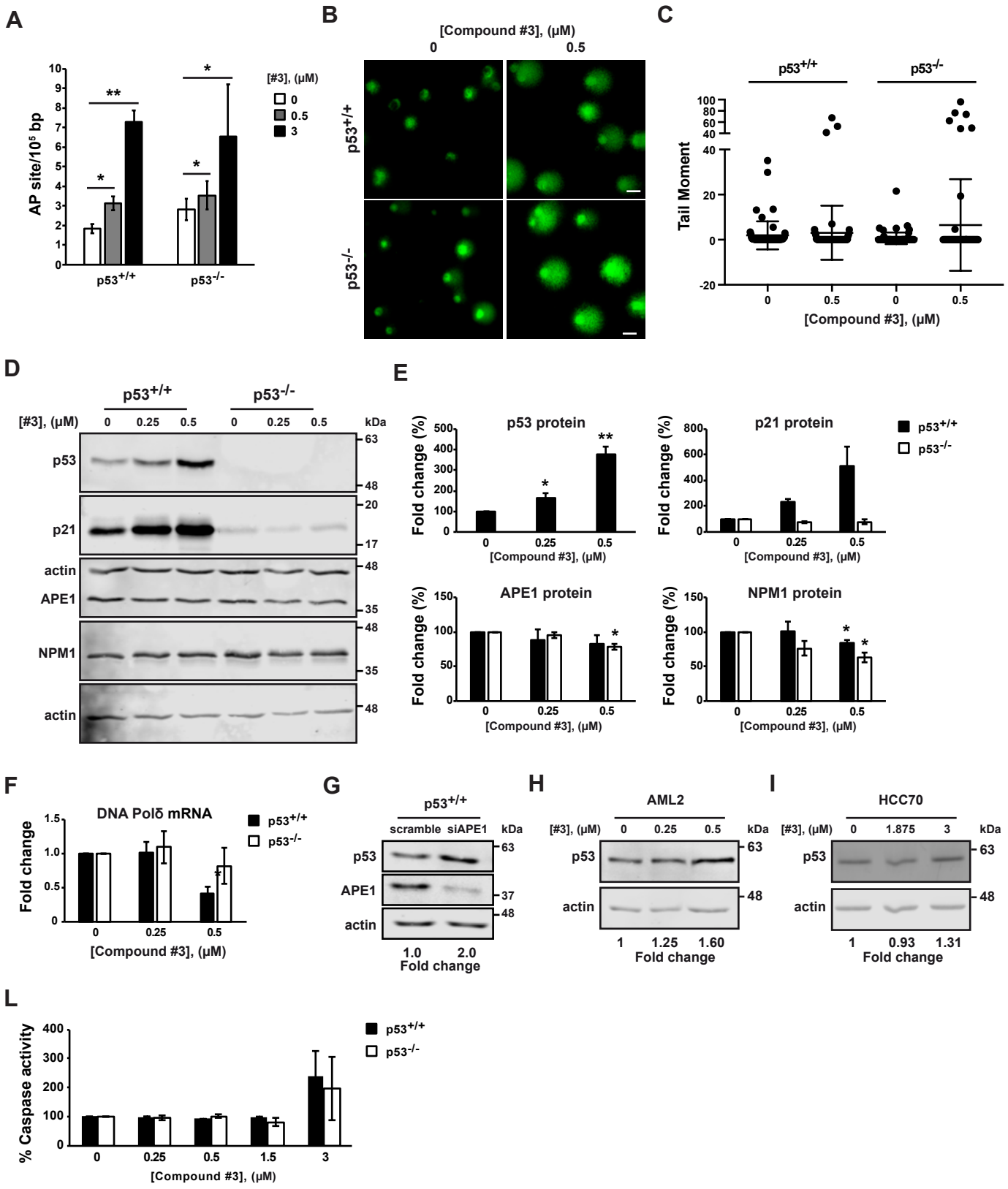
A
AP site/10^5 bp
[#3], (μM)
0
0.5
3
p53+/+
p53-/-
B
[Compound #3], (μM)
0
0.5
p53+/+
p53-/-
C
p53+/+
p53-/-
Tail Moment
[Compound #3], (μM)
D
p53+/+
p53-/-
[#3], (μM)
kDa
p53
p21
actin
APE1
NPM1
actin
E
p53 protein
p21 protein
APE1 protein
NPM1 protein
Fold change (%)
[Compound #3], (μM)
F
DNA Polδ mRNA
Fold change
[Compound #3], (μM)
G
p53+/+
scramble
siAPE1
p53
APE1
actin
Fold change
H
AML2
p53
actin
Fold change
I
HCC70
p53
actin
Fold change
L
% Caspase activity
[Compound #3], (μM)

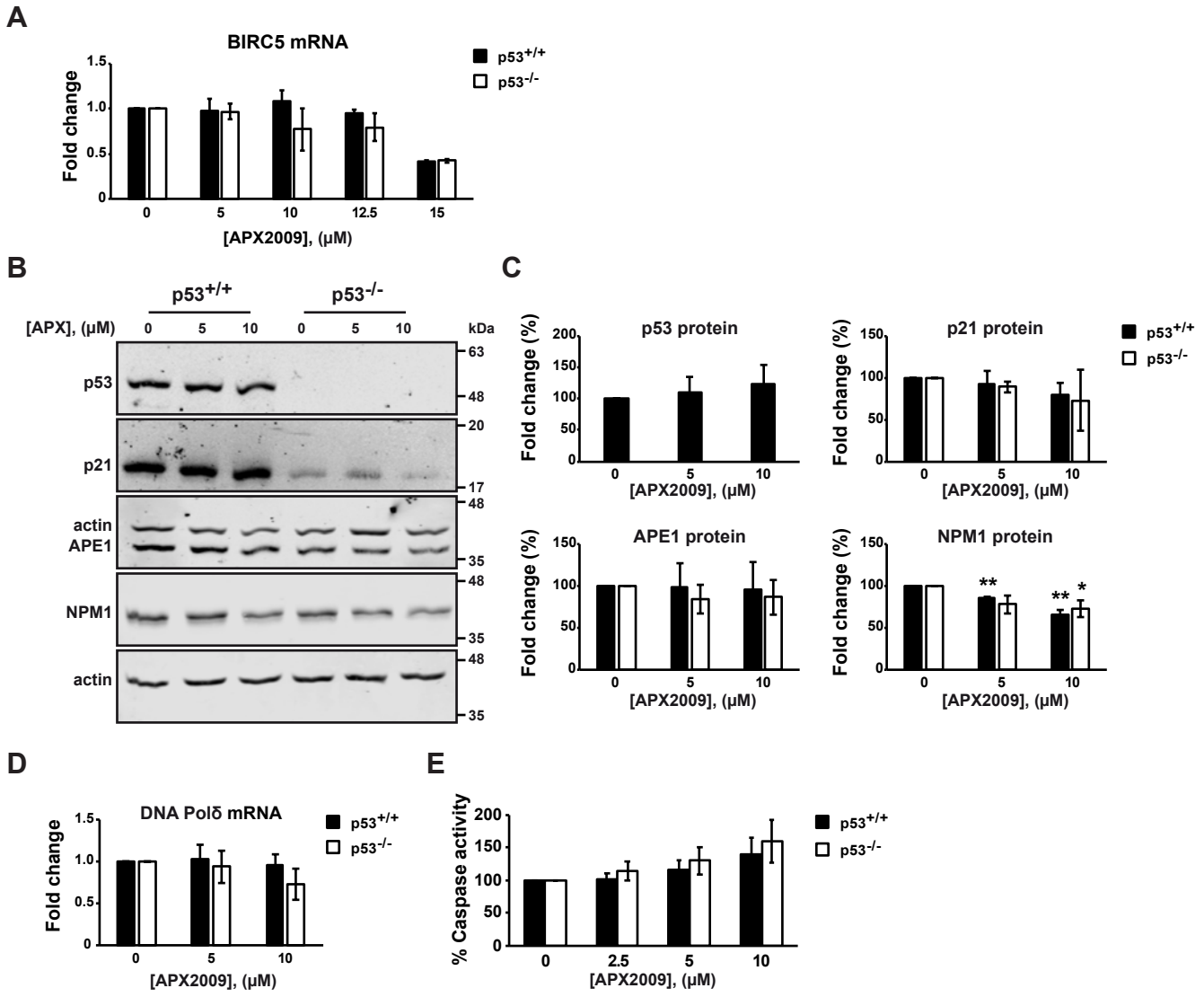
A
BIRC5 mRNA
p53+/+
p53-/-
Fold change
[APX2009], (μM)
B
p53+/+
p53-/-
[APX], (μM)
kDa
p53
p21
actin
APE1
NPM1
actin
C
p53 protein
p21 protein
APE1 protein
NPM1 protein
Fold change (%)
[APX2009], (μM)
D
DNA Polδ mRNA
E
% Caspase activity

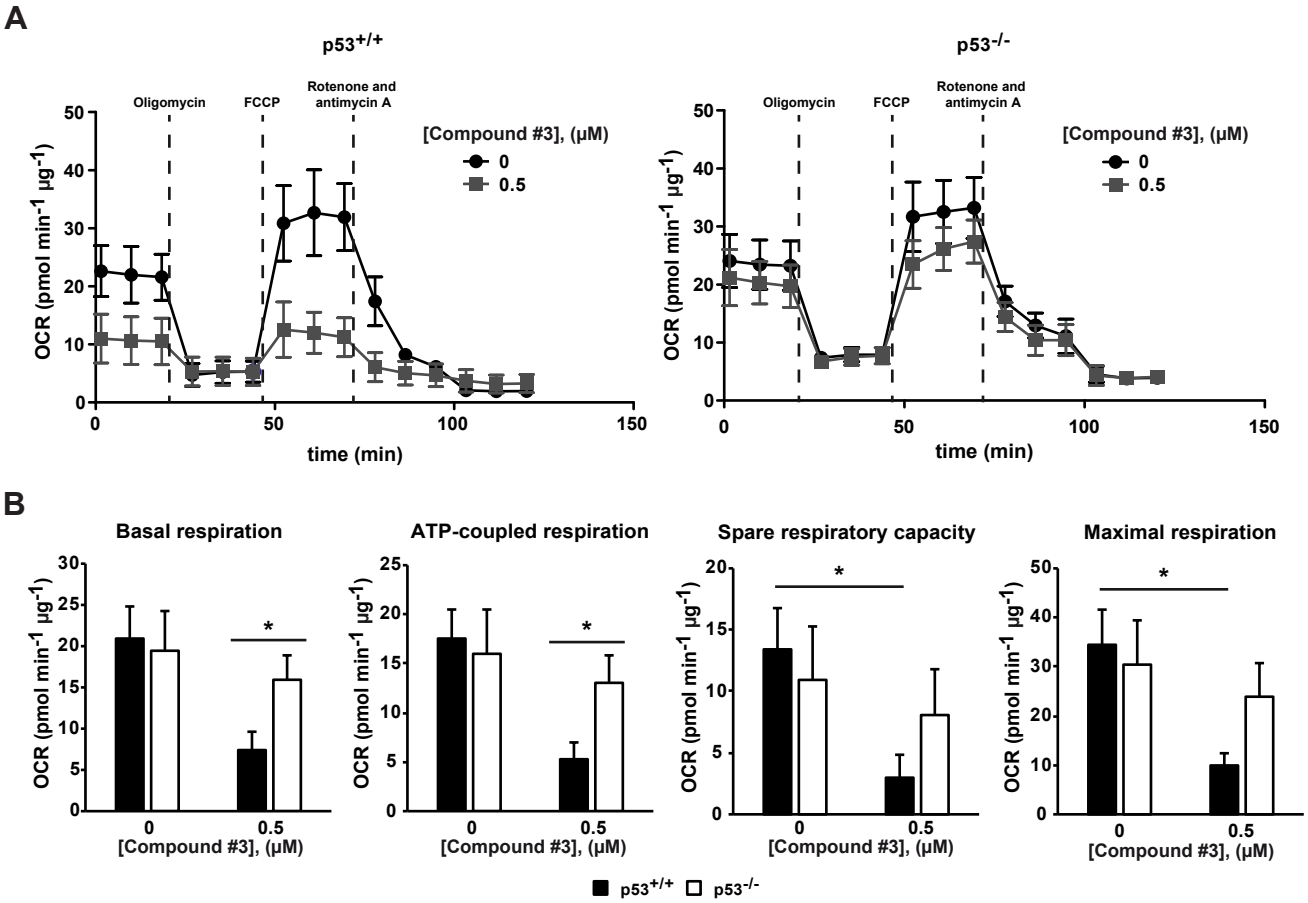
A
p53+/+
p53-/-
Oligomycin
FCCP
Rotenone and antimycin A
[Compound #3], (μM)
0
0.5
OCR (pmol min-1 μg-1)
time (min)
B
Basal respiration
ATP-coupled respiration
Spare respiratory capacity
Maximal respiration
[Compound #3], (μM)
p53+/+
p53-/-

Figure 5

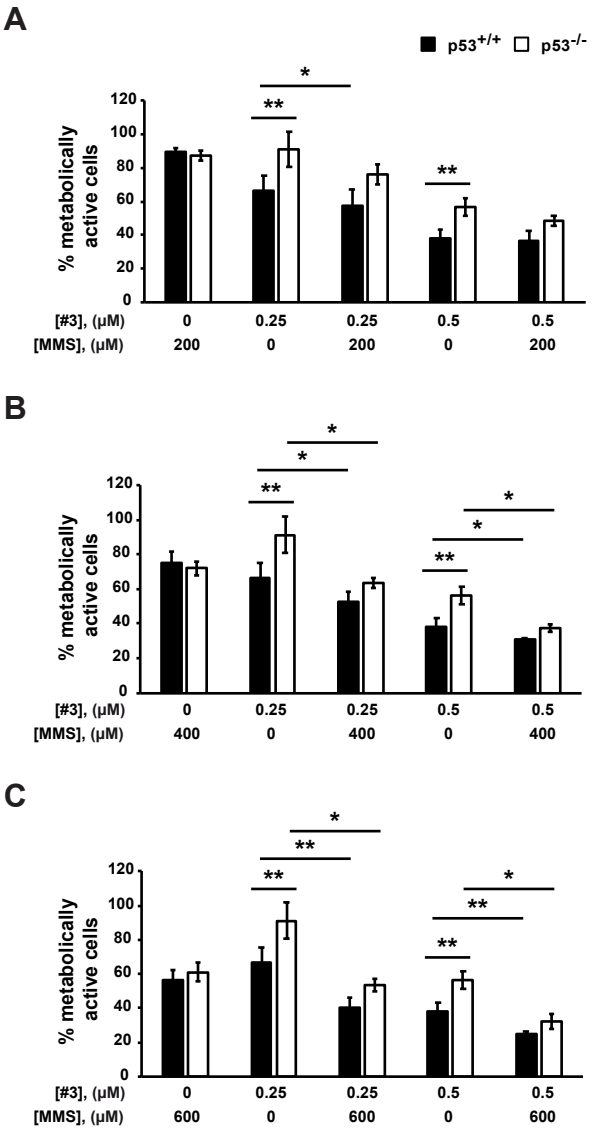
A
p53+/+
p53-/-
% metabolically active cells
120
100
80
60
40
20
0
*
**
**
[#3], (μM) 0 0.25 0.25 0.5 0.5
[MMS], (μM) 200 0 200 0 200
B
% metabolically active cells
*
*
**
*
*
**
[#3], (μM) 0 0.25 0.25 0.5 0.5
[MMS], (μM) 400 0 400 0 400
C
% metabolically active cells
*
**
**
*
**
**
[#3], (μM) 0 0.25 0.25 0.5 0.5
[MMS], (μM) 600 0 600 0 600

Figure 6

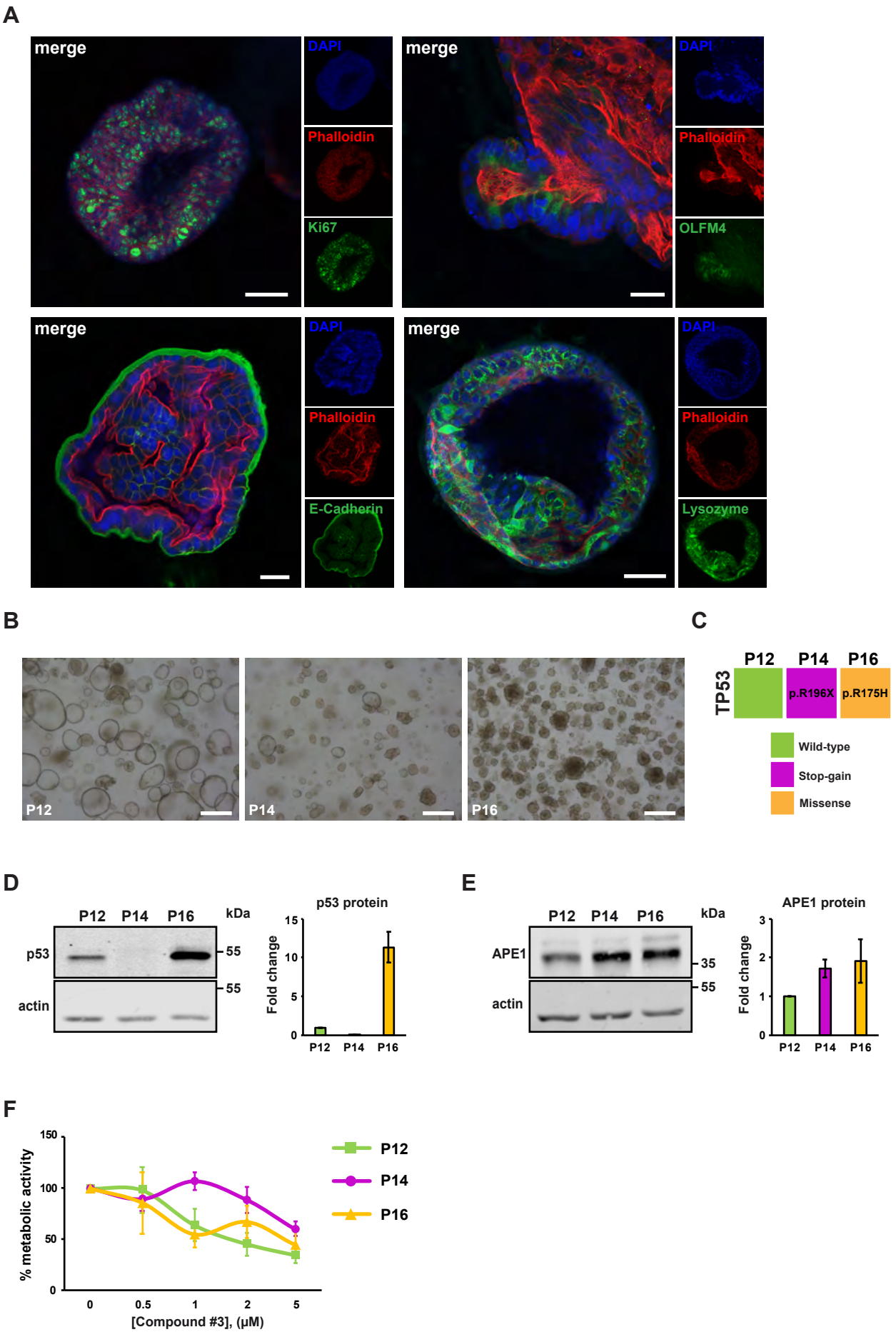
A
merge
DAPI
Phalloidin
Ki67
merge
DAPI
Phalloidin
OLFM4
merge
DAPI
Phalloidin
E-Cadherin
merge
DAPI
Phalloidin
Lysozyme
B
P12
P14
P16
C
TP53
P12
P14
P16
p.R196X
p.R175H
Wild-type
Stop-gain
Missense
D
P12
P14
P16
kDa
p53
actin
55
55
p53 protein
Fold change
15
10
5
0
P12
P14
P16
E
P12
P14
P16
kDa
APE1
actin
35
55
APE1 protein
Fold change
3
2
1
0
P12
P14
P16
F
% metabolic activity
150
100
50
0
0
0.5
1
2
5
[Compound #3], (μM)
P12
P14
P16

Figure 7

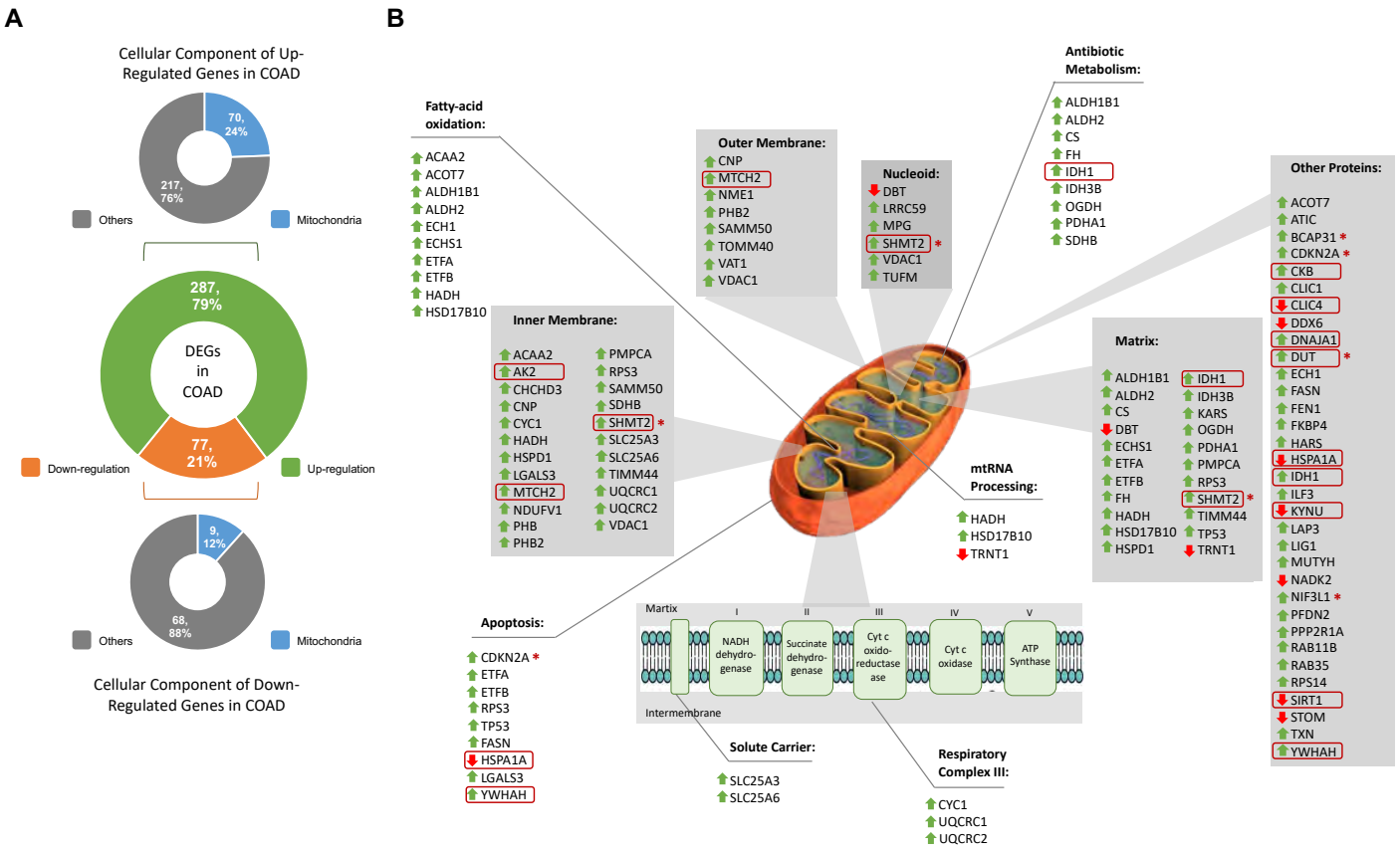
A
Cellular Component of Up-Regulated Genes in COAD
70, 24%
217, 76%
Others
Mitochondria
287, 79%
DEGs in COAD
77, 21%
Down-regulation
Up-regulation
9, 12%
68, 88%
Others
Mitochondria
Cellular Component of Down-Regulated Genes in COAD
B
Fatty-acid oxidation:
ACAA2
ACOT7
ALDH1B1
ALDH2
ECH1
ECHS1
ETFA
ETFB
HADH
HSD17B10
Outer Membrane:
CNP
MTCH2
NME1
PHB2
SAMM50
TOMM40
VAT1
VDAC1
Nucleoid:
DBT
LRRC59
MPG
SHMT2 *
VDAC1
TUFM
Antibiotic Metabolism:
ALDH1B1
ALDH2
CS
FH
IDH1
IDH3B
OGDH
PDHA1
SDHB
Other Proteins:
ACOT7
ATIC
BCAP31 *
CDKN2A *
CKB
CLIC1
CLIC4
DDX6
DNAJA1
DUT *
ECH1
FASN
FEN1
FKBP4
HARS
HSPA1A
IDH1
ILF3
KYNU
LAP3
LIG1
MUTYH
NADK2
NIF3L1 *
PFDN2
PPP2R1A
RAB11B
RAB35
RPS14
SIRT1
STOM
TXN
YWHAH
Inner Membrane:
ACAA2
AK2
CHCHD3
CNP
CYC1
HADH
HSPD1
LGALS3
MTCH2
NDUFV1
PHB
PHB2
PMPCA
RPS3
SAMM50
SDHB
SHMT2 *
SLC25A3
SLC25A6
TIMM44
UQCRC1
UQCRC2
VDAC1
Matrix:
ALDH1B1
ALDH2
CS
DBT
ECHS1
ETFA
ETFB
FH
HADH
HSD17B10
HSPD1
IDH1
IDH3B
KARS
OGDH
PDHA1
PMPCA
RPS3
SHMT2 *
TIMM44
TP53
TRNT1
mtRNA Processing:
HADH
HSD17B10
TRNT1
Apoptosis:
CDKN2A *
ETFA
ETFB
RPS3
TP53
FASN
HSPA1A
LGALS3
YWHAH
Martix
I
II
III
IV
V
NADH dehydro-genase
Succinate dehydro-genase
Cyt c oxido-reductase ase
Cyt c oxidase
ATP Synthase
Intermembrane
Solute Carrier:
SLC25A3
SLC25A6
Respiratory Complex III:
CYC1
UQCRC1
UQCRC2

Figure S1

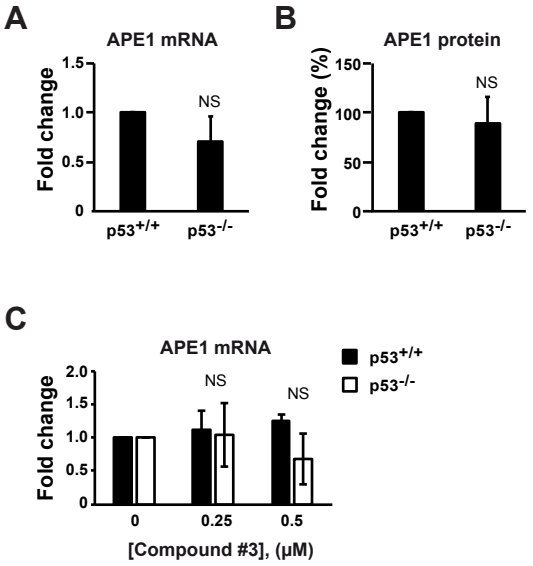
A
APE1 mRNA
Fold change
1.5
1.0
0.5
0
NS
p53+/+
p53-/-
B
APE1 protein
Fold change (%)
150
100
50
0
NS
p53+/+
p53-/-
C
APE1 mRNA
Fold change
2.0
1.5
1.0
0.5
0
NS
NS
0
0.25
0.5
[Compound #3], (μM)
p53+/+
p53-/-

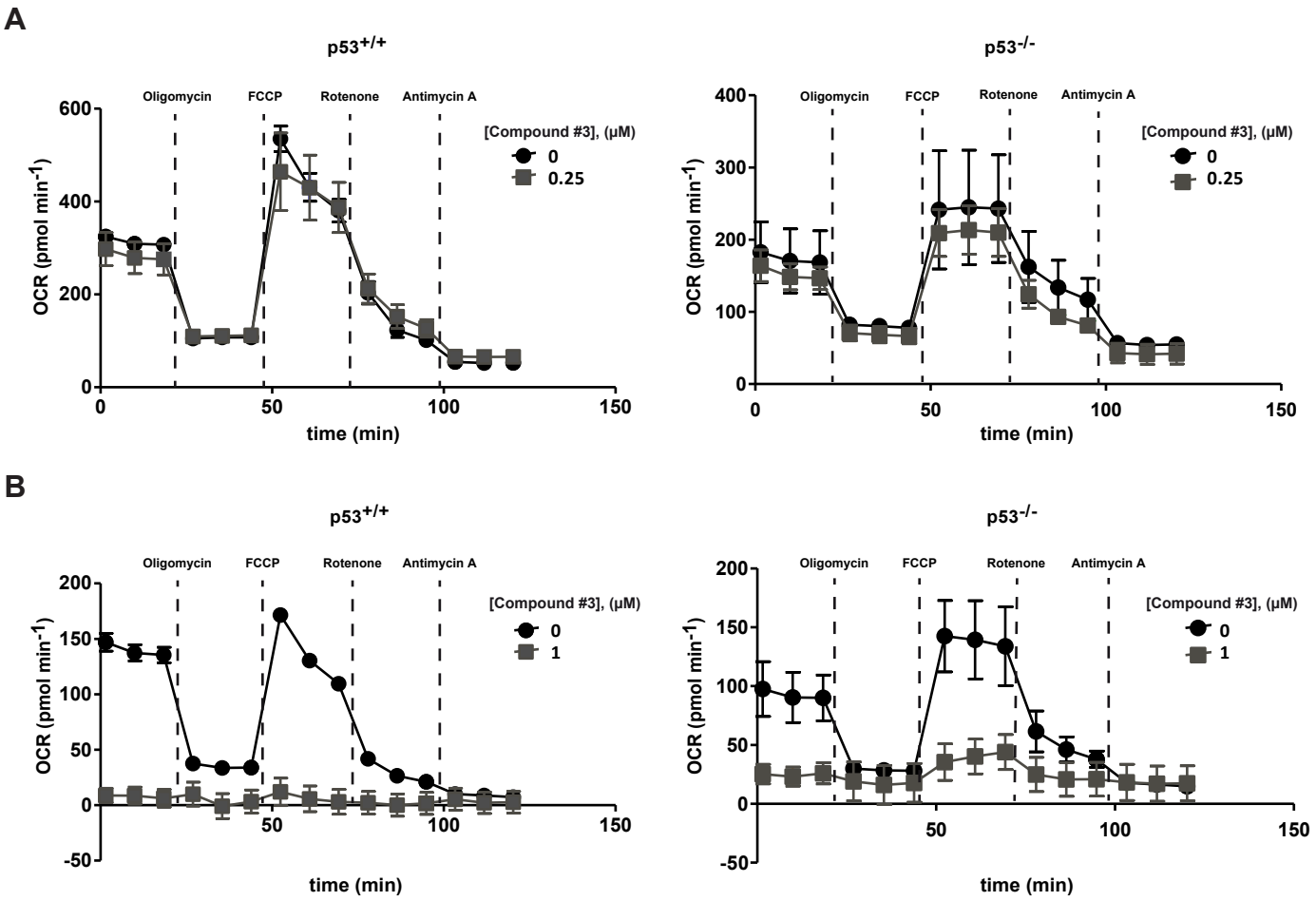
A
p53+/+
Oligomycin
FCCP
Rotenone
Antimycin A
[Compound #3], (μM)
0
0.25
OCR (pmol min-1)
time (min)
p53-/-
B
p53+/+
[Compound #3], (μM)
0
1
p53-/-